NAR Cancer, 2024, **6**, zcae039
https://doi.org/10.1093/narcan/zcae039
Advance access publication date: 3 October 2024
Cancer Gene Regulation, Chromatin, and Epigenetics

RNA kinetics influence the response to transcriptional perturbation in leukaemia cell lines

Izabela Todorovski [1,2], Mary-Jane Tsang[1,2], Breon Feran[3,4], Zheng Fan[1,2], Sreeja Gadipally[1], David Yoannidis[1], Isabella Y. Kong[3,4], Stefan Bjelosevic[1,2], Sarahi Rivera [3], Olivia Voulgaris[3], Magnus Zethoven [1], Edwin D. Hawkins[3,4], Kaylene J. Simpson[1,2], Gisela Mir Arnau[1,2], Anthony T. Papenfuss[1,2,3,4], Ricky W. Johnstone[1,2,*,†] and Stephin J. Vervoort[1,2,3,4,*,†]

[1]Peter MacCallum Cancer Centre, Melbourne, Victoria 3000, Australia
[2]Sir Peter MacCallum Department of Oncology, The University of Melbourne, Victoria 3010, Australia
[3]The Walter and Eliza Hall Institute of Medical Research, Parkville, Australia
[4]Department of Medical Biology, The University of Melbourne, Parkville, Australia

[*]To whom correspondence should be addressed. Tel: +61 39345 2892; Email: vervoort.s@wehi.edu.au
Correspondence may also be addressed to Ricky W. Johnstone. Tel: +61 85597133; Email: ricky.johnstone@petermac.org
[†]The last two authors should be regarded as Joint Last Authors.

Abstract

Therapeutic targeting of dysregulated transcription has emerged as a promising strategy for the treatment of cancers, such as leukaemias. The therapeutic response to small molecule inhibitors of Bromodomain-Containing Proteins (BRD), such as BRD2 and BRD4, P300/cAMP-response element binding protein (CBP) and Cyclin Dependent Kinases (CDKs), is generally attributed to the selective disruption of oncogenic gene expression driven by enhancers, super-enhancers (SEs) and lineage-specific transcription factors (TFs), including the *c-MYC* oncogene. The selectivity of compounds targeting the transcriptional machinery may be further shaped by post-transcriptional processes. To quantitatively assess the contribution of post-transcriptional regulation in responses to transcription inhibition, we performed multi-omics analyses to accurately measure mRNA production and decay kinetics. We demonstrate that it is not only the selective disruption of mRNA production, but rather mRNA decay rates that largely influence the selectivity associated with transcriptional inhibition. Accordingly, genes down-regulated with transcriptional inhibitors are largely characterized by extremely rapid mRNA production and turnover. In line with this notion, stabilization of the *c-MYC* transcript through swapping of its 3′ untranslated region (UTR) rendered *c-MYC* insensitive to transcriptional targeting. This failed to negate the impact on *c-MYC* downstream targets and did not abrogate therapeutic responses. Finally, we provide evidence that modulating post-transcriptional pathways, such as through ELAVL1 targeting, can sensitize long-lived mRNAs to transcriptional inhibition and be considered as a combination therapy approach in leukaemia. Taken together, these data demonstrate that mRNA kinetics influence the therapeutic response to transcriptional perturbation and can be modulated for novel therapeutic outcomes using transcriptional agents in leukaemia.

Graphical abstract

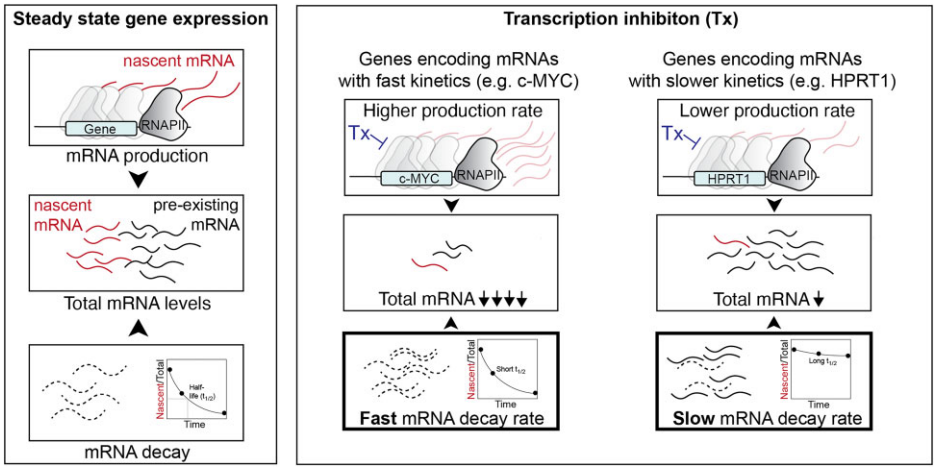

Received: April 11, 2023. **Revised:** July 30, 2024. **Editorial Decision:** September 9, 2024. **Accepted:** September 13, 2024

Introduction

Genetic alterations in cancer affect proteins involved in almost all regulatory steps of RNA Polymerase II (RNAPII)-driven gene expression. Dysregulated transcription ultimately contributes to cellular transformation and the development of malignant phenotypes (1,2). This includes leukaemias, where several chromosomal rearrangements, such as those involving the Mixed Lineage Leukemia (MLL) H3K4 methyltransferase, can drive the aberrant expression of leukaemogenic proteins (3). In addition to transcriptional and epigenetic changes, proteins involved in post-transcriptional processes, namely RNA binding proteins (RBPs), can similarly drive cancer progression (4). RBPs control the fate of RNAs by modulating their processing, localization and stability, and translation (5). This includes ELAV Like RNA binding protein 1 (ELAVL1)/ Human Antigen R (HuR), an RBP that plays a role in RNA stability by associating to introns and AU-rich regions in the mRNA 3′ untranslated regions (UTRs) (6–10). Importantly, ELAVL1 is overexpressed in various leukaemia types (11–13) and has recently been demonstrated to be necessary for leukaemic stem cell propagation *in vivo* (14).

Transcriptionally dysregulated cancers exhibit a critical dependency on proteins and complexes that control RNAPII. This observation has motivated the development of small molecule inhibitors of RNAPII regulators for therapeutic use (15,16). In leukaemia, this includes compounds that target the transcriptional co-activator p300/cAMP-response element binding protein (CBP), bromodomain and extra terminal (BET) family of epigenetic reader proteins such as bromodomain-containing protein 4 (BRD4) and transcriptional cyclin-dependent kinases (t-CDKs) (16–21). Several publications studying the effects of such small molecule inhibitors have shown that they result in selective gene expression responses. This selectivity is generally attributed to gene-specific chromatin features, including occupancy of the targeted factor, cell-type specific core regulatory transcription factors (CR-TFs), enhancers and super-enhancers (SEs) (1,22,23). In the context of leukaemia, this has been described to primarily affect oncogenic networks driven by key TFs such as *c-MYC* (23–26). Indeed, the sensitivity of *c-MYC* itself to transcriptional perturbation has largely been associated with a cluster of SEs located 1.7 mega bases (Mb) from its transcription start site (TSS) and CR-TFs such as PU.1, MYB and FLI1 (25,27). Unlike the selective disruption of enhancer activity observed upon small molecule targeting and acute depletion of p300/CBP and BRD4, perturbation of t-CDKs in contrast elicits a more global shutdown of transcription (22). Similar to t-CDK targeting, prolonged BRD4 degradation via the proteolysis-targeting chimera (PROTAC) molecule dBET6 has also been demonstrated to down-regulate nascent transcription genome-wide (28). Although selective targeting on chromatin may explain in part the gene expression response to transcriptional inhibitors, it does not fully clarify the differential sensitivity observed at the mRNA level, in particular in response to t-CDK targeting.

We set out to investigate how post-transcriptional regulation shapes the mRNA response to transcription inhibition. To this end, we leveraged recent technological advances that enable the accurate transcriptome-wide measurement of mRNA production and decay rates. This involves metabolic labelling of RNA with the nucleotide analogue 4-thiouridine (4sU) and its quantification using affinity- or conversion-based technologies such as thiol (SH)-linked alkylation for the metabolic sequencing of RNA (SLAM-seq) (29). We demonstrate that transcript decay rates, in combination with production rates, largely influence the response to transcriptional and epigenetic perturbation. Importantly, transcripts that are selectively down-regulated by transcriptional inhibitors are generally highly produced and short-lived transcripts and often encode genes regulated by CR-TFs and SEs. We further highlight that targeting the RBP ELAVL1 can sensitize long-lived transcripts to transcription inhibition and can provide enhanced anti-cancer responses.

Materials and methods

Cell lines and culture

K562 CML parental and HDR-edited and THP-1 AML parental and inducible knockout cells were cultured in Roswell Park Memorial Institute (RPMI) medium (Thermo Fisher Scientific, Waltham, MA, USA, 11875093) containing 10% (v/v) heat-inactivated fetal bovine serum (HI-FBS; Thermo Fisher Scientific, 10099), penicillin (100 U/ml), streptomycin (100 μg/ml) (Thermo Fisher Scientific, 15140122) and 2 mM GlutaMAX (Thermo Fisher Scientific, 35050061) at 37°C and 5% carbon dioxide. HEK293T cells were cultured in Dulbecco's modified Eagle's medium (DMEM; Thermo Fisher Scientific, 11995073) containing 10% (v/v) heat-inactivated fetal bovine serum (HI-FBS; Thermo Fisher Scientific, 10099), penicillin (100 U/ml) and streptomycin (100 μg/ml) (Thermo Fisher Scientific, 15140122) at 37°C and 10% carbon dioxide. *Drosophila melanogaster* S2 cells were cultured Schneider's *Drosophila* medium (Thermo Fisher Scientific, 21720) supplemented with 10% HI-FBS, penicillin (100 U/ml), streptomycin (100 μg/ml) and 2 mM GlutaMAX at room temperature and atmospheric carbon dioxide. Cell lines for all assays were seeded at 50–70% confluency the day prior unless otherwise indicated.

Compounds

See Supplementary Tables S1 and S2.

Generation of ELAVL1 inducible knockout cell lines

Independent sgRNAs targeting ELAVL1 and non-targeting sgRNA controls (SCR; Supplementary Table S3) flanked with BsmBI overhangs were ligated into the vector FgH1tUTG-GFP (Addgene Plasmid #70183) using 1uL BsmBI (New England Biolabs, R0739) in NEBuffer 3.1 (New England Biolabs, B7203S). This was similarly performed for SCR sgRNA cloned into the vector FgH1tUTG-BFP (47). Cloned FgH1tUTG vectors, pMDLg/pRRE (Addgene Plasmid #12251), pRSV-Rev (Addgene Plasmid #12253) and pVSV.G (Addgene Plasmid #12259) third generation lentiviral vectors were transiently transfected into HEK293T cells using polyethylenimine (PEI; 1 μg/ml; 25kD linear; BioScientific Pty Ltd, 23966). Following 48 h, viral supernatant was harvested and filtered using a 0.45 μM filter. Viral supernatant was added THP-1 cells constitutively expressing *S. pyogenes* Cas9 (FUCas9-Cherry vector; Addgene Plasmid #70812) prior to transduction using sequa-brene (4 μg/ml; Sigma Aldrich, S2667-1VL) and centrifugation at 500g for 4 min at room temperature (47). Expanded cells were sorted for populations expressing cherry and GFP or BFP using Becton Dickinson (BD) Fussion 3 or 5 sorters. sgRNA expression was induced using doxycycline (1μg/ml; Sigma Aldrich, D9891).

All experiments were performed 4 days following doxycycline induction unless otherwise indicated.

CRISPR HDR generation of MYC transcript stable clones

Parental K562 cells (5e + 05) were washed in Phosphate Buffered Saline (PBS) twice and resuspended in Cell Line Nucleofector solution SF (16.4 ul) with Supplement (3.6 ul) (SF Cell Line 4D-nucleofector X Kit, Lonza, V4XC-2032). Alt-R SpCas9 nuclease (100pmol, Integrated DNA Technologies, 1074182), single guide RNAs (sgRNAs) targeting the c-MYC stop codon and 3′ end of its 3′UTR (300 pmol, Supplementary Table S3) and pUC57 or pUC57-Mini donor plasmid (1000 ng; GenScript Gene Sythesis) containing recombinant sequences for dGFP, P2A cleavable peptide and HPRT1 or c-MYC 3′UTRs, respectively (Supplementary Table S4), were incubated together for 20 min at room temperature, prior to being placed on ice. Ribonucleoprotein (RNP) complex (5 ul) was added to the cell suspension (20 ul), 20 ul of which was subsequently transferred to 16-well Nucleocuvette Strip and electroporated using the 4D-Nuceleofector X unit (program FF120, Lonza, AAF-1002X). Warmed culture medium (100 ul) was added to cell suspension and incubated at 37°C and 5% carbon dioxide for 10 min. Cell suspension was then transferred to a 24-well cell culture plate containing culture medium (1 ml) and IDT Alt-R HDR electroporation enhancer (20 uM; Integrated DNA Technologies, 1081073) and incubated at 37°C and 5% carbon dioxide for 24 h, after which cells were washed twice with fresh culture medium and cultured at 37°C and 5% carbon dioxide. After expansion, cells were sorted and enriched for GFP positivity three successive times, followed by isolation of single cells into 96-well culture plates using Becton Dickinson (BD) FACSAria Fusion 3 or 5 Cell Sorters. Three clones with successful knock in of each donor vector were identified with KAPA HiFi (Roche, 7958935001) using isolated genomic DNA (DNeasy Blood & Tissue Kits (Qiagen, 69506) and primers designed outside or within plasmid homology arms (Supplementary Table S5). PCR fragments were subsequently separated using agarose gel electrophoresis (see below). Knock-in sequence was validated using Sanger sequencing of PCR fragments detailed above at the Australian Genome Research Facility (AGRF). Total-RNA sequencing was performed using a single representative clone of each knock-in.

Propidium iodide, 4′,6-diamidino-2-phenylindole and cell Trace violet staining

For cell viability and proliferation studies using propidium iodide (PI) and/or Cell Trace Violet staining, respectively, cells (1×10^7) were centrifuged (500g at 4°C for 4 min), resuspended in PBS supplemented with 0.1% (w/v) BSA and stained with 5 μM CTV dye (Thermo Fisher Scientific, C34557) in a 37°C water bath for 10 or 20 min. Five volumes of ice-cold culture medium was added to cell suspension to quench unbound dye. Cells were then centrifuged (500g at 4°C for 4 min), resuspended in PBS supplemented with 2% (v/v) HI-FBS, sorted for a narrow peak of CTV-positivity on BD FACSAria Fusion 3 or 5 Cell Sorters. Following treatment, CTV-stained or unsustained cells were resuspended in PBS containing 1 μg/ml PI (Sigma Aldrich, P4170).

For cell viability studies using 4′,6-diamidino-2-phenylindole (DAPI), cells were treated with AZ-5576 (CDK9i) for 72 h, centrifuged (500g at 4°C for 4 min) and resuspended in PBS containing 1 μg/ml DAPI (Sigma Aldrich, D9542-100MG). Analysis of flow cytometric data was preformed using the BD Fortessa X20 and FlowJo v10 software (Ashland). ZIP synergy scores were determined and visualized using synergyfinder (v3.0.1) on Rstudio (v4.0.2).

All experiments were performed in three biological repeats unless stated otherwise.

CellTiter-glo viability assessment

THP-1 cells were diluted to 0.35×10^6 cells/ml and cultured overnight before seeding with 2-fold dilution in 96-well plate with the indicated concentrations of AZ-5576 (CDK9i) and MS-444. After a further 72 h incubation, 50ul cells were mixed 1:1 with 50 ul CellTiter-Glo® 2.0 Reagent (Promega, G9243) with 2 min agitation for cell lysis and an additional 10 min incubation. Luminescence was recorded on BioTek Cytation 5 (Agilent) with Gain set to 125. All experiments were performed in three biological repeats.

Total cell number quantification

Absolute cell number was determined with the addition of 1×10^4 calibration beads directly to cells prior to analysis. 0.2 μM propidium iodide (PI) was also added with the beads to identify dead cells by exclusion. Ratio of live cells to beads was measured by flow cytometry to determine the absolute live cell number in cell culture. All experiments were performed in three biological repeats.

Intracellular staining of c-MYC

Intracellular staining of Myc was performed as previously described (60). Briefly, cells were harvested at the timepoints indicated and were immediately resuspended in fixation buffer (0.5% paraformaldehyde, 0.2% Tween-20 and 0.1% bovine serum albumin in PBS) at room temperature, for at least 24 h until staining was performed. Fixed cells were stained with either anti-Myc (clone D84C12, Cell Signalling Technology) or a rabbit IgG isotype-matched control antibody (clone D1AE, Cell Signalling Technology) before staining with an anti-rabbit IgG conjugated to Alexa Fluor 647. Staining of all fixed samples within one experiment was performed at the same time. All experiments were performed in two biological repeats.

Cell competition assays

Four days after induction of sgRNA using doxycycline (1 μg/ml; Sigma Aldrich, D9891), THP-1 Cas9 cells expressing FgH1tUTG-GFP constructs were mixed at a 1:1 ratio with THP-1 Cas9 cells expressing a SCR sgRNA in the FgH1tUTG-BFP backbone. Cells were cultured in the presence of DMSO or AZ'5576 (CDK9i; 10nM and 100nM). The BD LSR Fortessa Flow Cytometer was used to assess the relative proportions of GFP- and BFP-positive cells following mixing (time point 0) and at time points indicated. All experiments were performed in three biological repeats.

Agarose gel electrophoresis and gel imaging

Blue/orange loading dye 6X (Promega, G1881) was added to PCR fragments, which were subsequently separated using 1% agarose gels prepared with molecular grade agarose (Bioline, BIO-41025), Tris base–acetic acid–EDTA (TAE) 1× solution and SYBR Safe DNA Gel Stain (Life Technologies,

S33102). Agarose gels were imaged on the GelDoc XR + Imager (BioRad) using ImageLab Software (BioRad). All experiments were performed in three biological repeats.

Quantitative PCR and analysis

Cells (1e + 06 per time point) were incubated with 1ug/ml ACTD at 37°C and 5% carbon dioxide, harvested 0-, 2-, 4- and 8-h post-treatment, centrifuged (1400 rpm at 4°C for 4 min), washed in ice-cold PBS and resuspended in 300 ul TRIzol (Thermo Fisher Scientific, 15596026). RNA was extracted from lysates using the Direct-zol RNA MiniPrep Kit (Zymo Research, R2052) and complimentary DNA (cDNA) was synthesized (from 1ug RNA) using the Applied Biosystems High Capacity cDNA Reverse Transcription Kit (Thermo Fisher Scientific, 4368814). Quantitative PCR (qPCR) was performed using cDNA, 0.25uM forward and reverse oligo primers (see Supplementary Table S6) and SensiFAST SYBR Hi-ROX Kit (Bioline, BIO-92005) in 384-well plates with the LightCycler 480 Instrument II (Roche, 05015243001). Threshold cycles for each reaction were analysed using the $\Delta\Delta C_t$ method normalizing to GAPDH as the housekeeping gene. All experiments were performed in three biological repeats.

SDS-polyacrylamide gel electrophoresis and western blotting

Cells (1e + 06) were washed in PBS, lysed in Laemelli Buffer (60 mM Tris–HCl (pH 6.8), 10% (v/v) glycerol and 2% (w/v) SDS) and incubated at 95°C for 10 min. Lysate protein concentration was determined using the Pierce BCA Protein Assay Kit (Thermo Fisher Scientific, 23225) and absorbance at 562 nm wavelength was measured on the iMark Microplate Absorbance reader (BioRad) using MicroPlate Manager Software (BioRad). 20× sample buffer (100% β-mercaptoethanol, and bromophenol blue) was added to lysates and were subsequently incubated for an additional 5 min. Lysates were separated using Mini-PROTEAN TGX 4 to 15% gradient gels (25 mM Tris, 192 mM glycine and 0.1% (w/v) SDS; Bio-Rad, 4561086) and transferred at 4°C to either Immobilon-FL or Immunoblon-P (IPVH00010) polyvinylidene fluoride membranes (Merck, IPFL00010) (1.5 h; 250 mA, 25 mM Tris, 192 mM glycine and 5% (v/v) methanol).

Immobilon-FL membranes were dried for 1 hour at room temperature, washed in ultrapure water, 100% methanol, Tris buffered saline (TBS) in the listed order and blocked using Odyssey blocking buffer (Li-COR, 927-40000). They were then incubated in primary antibodies (Supplementary Table S7) diluted in Odyssey blocking buffer supplemented with 0.2% (v/v) Tween 20 (Sigma-Aldrich, P9416) overnight at 4°C, washed three times with TBS containing 0.1% (v/v) Tween 20 and incubated with IRDye-conjugated secondary antibodies (Supplementary Table S7) diluted in Odyssey blocking buffer supplemented with 0.2% (v/v) Tween 20 and 10% (v/v) sodium dodecyl sulfate (SDS) for 1 h at room temperature. Immobilon-FL membranes were washed in PBS and protein was visualized and quantified using the Odyssey CLx and Image Studio Lite software 2 (Li-COR).

Immunoblon-P membranes were blocked in TBS supplemented with 5% (w/v) skim milk powder and Tween 20, incubated with primary antibodies (Supplementary Table S7) diluted in the same solution at 4°C overnight, washed three times with TBS containing 0.1% (v/v) Tween 20 and incubated with horseradish peroxidase-conjugated secondary antibodies (Supplementary Table S7) at room temperature for 1 h. Protein was subsequently visualized using Amersham ECL Plus (GE Healthcare, RPN2132) and Super RX film (Fujifilm, 03G01). All experiments were performed in three biological repeats.

Total RNA-sequencing

Cells (1e + 06^6 per treatment condition) were centrifuged (1400 rpm at 4°C for 4 min), washed in ice-cold PBS and resuspended in 350 µl of Buffer RLT Plus supplemented with 1% (v/v) β-mercaptoethanol from the RNeasy Plus Mini Kit (Qiagen, 74134). RNA was extracted using the same kit according to manufacturer's instructions and quality was assessed using the Agilent 2200 TapeStation System (Agilent, G2964AA) with RNA ScreenTape (Agilent, 5067–5576) and Sample Buffer (Agilent, 5067-5577). S2 spike-in material (5%) was added to RNA. Sequencing libraries were prepared using NEBNext Ultra II Directional RNA Library Prep Kit for Illumina, where ribodepletion was performed using the NEBNext rRNA Depletion Kit (New England BioLabs, E6310). Paired-end 75 bp reads were sequenced using the NextSeq 500 (Illumina). All experiments were performed in two technical repeats.

3′UTR-sequencing

Cells were treated with DMSO or AZ-5576 (CDK9i; 100 nM) for 6 h at 37°C and 5% carbon dioxide. Following incubation, cells were harvested, centrifuged (500g at 4°C for 4 min), washed in ice-cold PBS and resuspended in 600 µl TRIzol. RNA was extracted using the Directzol RNA Miniprep Kit, where an additional DNase I digestion step was performed (Zymogen; R2052). Sequencing libraries were prepared using the QuantSeq 3′mRNA-seq Library Prep Kit FWD for Illumina (Lexogen, Vienna, Austria) and sequenced as single-end 75 bp reads using the NextSeq 500 (Illumina). All experiments were performed in two technical repeats.

SLAM-sequencing

Protocol was adapted from (18). K562 and THP-1 cells (1e + 06 per treatment) were first pre-treated with small molecule inhibitors for a total time of 2 h to pre-establish protein-target inhibition. Newly synthesized RNA in K562 cells was then labelled using 100 µM 4-sU in the final 1 h of treatment at 37°C and 5% carbon dioxide. Cells were washed in ice-cold PBS and resuspended in 300 µl TRIzol. For direct measurement of RNA half-lives, newly synthesized RNA was labelled by incubating cells in 30 µM 4-sU for 12 h at 37°C and 5% carbon dioxide, whereby culture medium was exchanged every 3 h for the duration of the pulse. For the uridine chase, cells were centrifuged (1400 rpm at 4°C for 4 min), washed in sterile ice-cold PBS twice and resuspended in pre-warmed (37°C) culture medium containing 3mM uridine (Sigma Aldrich, U6381). At 0-, 1-, 2-, 4-, 8-, 12-h for K562 cells and 0-, 0.3-, 0.6-, 1-, 2-, 4-, 8-h for THP-1 cells post the uridine chase, cells were harvested, centrifuged (1400 rpm at 4°C for 4 min) and resuspended in 300 µl TRIzol. For treatment-specific RNA decay rates, cells were centrifuged (1400 rpm at 4°C for 4 min), washed in sterile ice-cold PBS

twice and resuspended in pre-warmed (37°C) culture medium containing 3 mM uridine (Sigma Aldrich, U6381) and either 1μM DMSO, JQ1 or AZ-5576. At 0-, 2-, 4- and 8-h post uridine chase/drug addition, cells for each treatment condition were harvested, centrifuged (1400 rpm at 4°C for 4 min) and resuspended in 300 μl TRIzol. All SLAM-seq experiments included a non-4-sU labelled control unless otherwise stated. To extract RNA, one-fifth volume of chloroform was added to TRIzol lysates, followed by shaking, incubation at room temperature for 2 min and centrifugation (16 000g at 4°C for 15 min). The aqueous phase was isolated and RNA was precipitated using DTT (10 mM), 100% isopropanol (1 volume) and GlycolBlue co-precipitant (15 ug, Ambion, AM9515), incubated at room temperature for 10 min and centrifuged (16 000g at 4°C for 20 min). Supernatant was removed, RNA pellets were washed in 75% (v/v) ethanol and DTT (100 μM) and centrifuged (7500g at room temperature for 5 min). Supernatant was removed and RNA pellets dried for 10 min prior to reconstitution in Ultrapure DNAse/RNAse-free distilled water (Thermo Fisher Scientific, 10977023) supplemented with DTT (1mM) and incubation at 55°C for 10 min. Thiol-containing bases were reduced by incubating RNA (10 μg) with IAA (10 mM, 50 mM $NaPO_4$ pH 8.05 and 50% (v/v) DMSO) in a final volume of 50 μl for 15 min at 55°C. Reaction was stopped by quenching IAA with DTT (20 μM). RNA was precipitated using 3 M NaOAc pH 5.2 (5 μl), 100% ethanol (125 μl) and GlycolBlue co-precipitant, incubated at −80°C for 30 min and centrifuged (16 000g at 4°C for 30 min). Supernatant was removed and RNA pellet was washed in 75% (v/v) ethanol and centrifuged (16 000g at 4°C for 10 min) twice, dried at room temperature for 10 min and reconstituted in Ultrapure DNAse/RNAse-free distilled water. RNA clean-up was performed by incubating RNA solution in 2 volumes of AMPure XP Beads (Beckman Coulter, A63881) for 2 min at room temperature. Beads were washed in 80% (v/v) ethanol twice, dried at room temperature for 3 min and resuspended in Ultrapure DNAse/RNAse-free distilled water. Eluate was collected and RNA quality and concentration was assessed using the Agilent 2200 TapeStation System (Agilent, G2964AA) with RNA ScreenTape (Agilent, 5067-5576) and Sample Buffer (Agilent, 5067-5577). S2 spike-in material (5%) was added to RNA. Sequencing libraries were prepared using the QuantSeq 3′mRNA-seq Library Prep Kit FWD for Illumina (Lexogen, Vienna, Austria) and sequenced as single-end 75 bp reads using the NextSeq 500 (Illumina). All experiments were performed in two technical repeats.

TT-sequencing

Protocol is adapted from (21). Cells (5e + 07 per treatment condition) were incubated with 1 mM 4sU for either 5 or 15 min at 37°C and 5% carbon dioxide, centrifuged (1400 rpm at 4°C for 5 min) and resuspended in TRIzol (5 ml). One-fifth volume of chloroform was added to lysates, followed by shaking, incubation at room temperature for 2 min and centrifugation (13000g at 4°C for 10 min). The aqueous phase was isolated and RNA was precipitated using 100% isopropanol (1 volume), incubated at room temperature for 10 min and centrifuged (13000 rpm at 4°C for 10 min). Supernatant was removed and RNA pellet was washed in 70% (v/v) ethanol, reconstituted in Ultrapure DNAse/RNAse-free distilled water (100μl) and denatured at 65°C for 10 min. S2 spike-in (15 μg) was added to RNA (150 μg), material was adjusted to a final volume 100μl and sonicated in microTUBE AFA Fiber screw cap tubes (6 mm × 16 mm, Covaris, 520096) using the Covaris S220 Focused-ultrasonicator at a maximum power for 15 seconds. Thiol-specific biotinylation of RNA was performed in a final volume of 1.5ml by incubation with 10 mM Tris (pH 7.4), 1 mM EDTA, 20% (v/v) dimethylformamide (200 μg/ml; Sigma-Aldrich, 227056), and 300 μg of EZ-Link HPDP-Biotin (Thermo Fisher Scientific, 21341) for 1.5 h at room temperature. An equal volume of chloroform was added to reaction, followed by shaking, incubation at room temperature for 2 min and centrifugation (1400 rpm at 4°C for 5 min). Aqueous phase was isolated and an equal volume of chloroform was added, followed by shaking, incubation at room temperature for 2 min and centrifugation (1400 rpm at 4°C for 5 min). This step was repeated an additional one time. Aqueous phase was isolated and RNA was precipitated using 5 M NaCl (10% volume) and 100% isopropanol (1 volume) and centrifugation (20 000g at 4°C for 20 min). RNA pellets were washed in 75% (v/v) ethanol, reconstituted in Ultrapure DNAse/RNAse-free distilled water (100 μl) and denatured at 65°C for 10 min. Biotinylated RNA was separated from the total RNA pool by incubation with streptavidin beads (μMACs Streptavidin Kit, Miltenyi Biotec, Bergisch Gladbach, Germany, 130-074-101) at room temperature for 15 min with constant rotation. μMACs columns pre-equilibrated with room temperature wash buffer (100 mM Tris–HCl (pH 7.4), 10 mM EDTA, 1 M NaCl, and 0.1% (v/v) Tween 20) were used to bind streptavidin beads, which were then washed using 900 μl wash buffer that was heated to 65°C or at room temperature, 5 times each. Biotinylated RNA was eluted into 700 μl Buffer RLT from the RNeasy MinElute Cleanup Kit (Qiagen, 74204) through two additions of 100 mM DTT (100 μl) 3 min apart, and then isolated using the same kit according to manufacturer's instructions. RNA concentration was quantified using the Agilent 2200 TapeStation System (Agilent, G2964AA) with High Sensitivity RNA ScreenTape (Agilent, 5067-5579) and Sample Buffer (Agilent, 5067-5580).

Sequencing libraries were prepared with the NEBNext Ultra II Directional RNA Library Prep Kit for Illumina (without additional fragmentation), where ribodepletion was performed using the NEBNext rRNA Depletion Kit (New England BioLabs, E6310). Single-end 75 base pair reads were sequenced using the NextSeq 500 (Illumina). All experiments were performed in two technical repeats.

MAC-seq

Cells (5e + 04 per well) in a final volume of 100 μl in a 96-well plate format were incubated with transcriptional and epigenetic inhibitors in technical duplicate for 6 h (Supplementary Table S8) at 37°C and 5% carbon dioxide. 5e + 03 cells from each well were aliquoted into a separate 96-well plate, washed in ice-cold PBS twice and centrifuged (1400 rpm at 4°C for 4 min). Supernatant was removed and cell pellets were frozen at −80°C. Library preparation is adapted from (61). In detail, 17 μl lysis buffer were added into each well of a 96-well plate containing cell pellets and incubated at room temperature for 15 min under agitation (900 rpm). 12.5 μl of cell lysate were transferred into each well of a new 96-well plate previously prepared with 1 μl of 10 nM well-specific RT MAC-seq primer and 7.5 μl RT mix; the RT mix contains a TSO primer and

external ERCC RNAs. The mixture was incubated for 2 h at 42°C to create well-barcoded full length cDNA and then all the wells of a plate were combined into a single tube. Concentration and clean-up was done via column purification (DNA Clean and Concentrator™-100, Zymo Research) and RNA-Clean XP beads (Beckman Coulter) and each plate eluted in 22 µl nuclease free water. The purified cDNA was pre-amplified with KAPA HiFi HotStart ReadyMix (Roche) and MAC-seq PreAmp PCR primer and the quality checked on a D5000 Screentape (TapeStation, Agilent). One barcoded library was prepared per plate using TD buffer and TDE1 enzyme (Illumina) for tagmentation and KAPA HiFi HotStart Ready Mix (Roche) and custom primers (MAC-seq P5 PCR and MAC-seq Indexing Mix) for amplification. Libraries were purified with DNA Ampure XP beads (Beckman Coulter), quality checked on a DNA1000 tape (TapeStation, Agilent) and quantity verified by qPCR. Two indexed libraries were sequenced on a NextSeq 500 instrument (Illumina) using a custom sequencing primer (MAC-seq Read primer) and a High Output Kit v2.5 75 Cycles (Illumina) with paired-end configuration (25 base pairs for read 1 and 50 bp for read 2). All experiments were performed in two technical repeats.

SLAM-seq analysis

Single-end reads were demultiplexed using bcl2fastq (v2.17.1.14) and resulting FASTQ files were trimmed for adapter sequences using Trim_galore (v0.6.5) with a stringency overlap of 3bp. Trimmed FASTQ files were processed with SLAM-dunk (v0.4.3), enabling multi-mapper reconciliation and using a threshold of at least 2 T > C conversions to mark a read as converted. The no 4sU control sample was processed first to find single nucleotide polymorphisms (SNPs), which was then used to filter the subsequent samples. 'bedtools merge' was then used to merge the 3′ UTRs of each Ensembl transcript by gene (v77 identifiers for hg38) for use in the SLAM-dunk counting step. The Broad Institute GSEA software was used to perform GSEA (62). Differential gene testing was performed on counts normalized to library sizes scaled to external S2 spike-ins and filtered for lowly expressed genes using edgeR (v3.32.1) on Rstudio (v4.0.2). SLAM sequencing tcount files from (30) (GEO accession GSE138210) and (11) (GEO accession GSE111463) were downloaded and differential gene testing was performed as described above.

TT-seq analysis

Single-end reads were demultiplexed using bcl2fastq (v2.17.1.14) and resulting FASTQ files were aligned to the genome using STAR (v2.7), which were then summarized using featureCounts in Subread (v2.0.1): counting reads with a minimum Mapping Quality Score (MQS) of 7 in the union of all transcript isoforms of each Ensembl gene. Only genes with at least 10 reads per million across at least two samples within an experiment were retained for further analysis. In order to compare expression levels between samples, raw read counts for each gene were converted to reads per million using adjusted library sizes calculated with edgeR's TMM implementation on the spike-in read counts.

Total RNA-seq analysis

Paired-end reads were demultiplexed using bcl2fastq (v2.17.1.14) and resulting FASTQ files were quality checked using fastqc (v0.11.6), trimmed 15 bp from the 5′ end to remove primer bias and filtered for quality and length using cutadapt (v2.1; -u 15 -U 15 -q 15 –pair-filter any –minimum-length 50). Trimmed reads were mapped to GRCh38/hg38 and BDGP6/dm6 genomes using hisat2 (v2.1.0) with paired read settings and resulting SAM files were converted to BAM files using samtools (v1.9; view), which were then sorted and indexed. Reads mapping to either exonic or intronic genomic intervals were counted using a combined hg38/dm6/GFP GTF file with FeatureCounts from the subread package (v2.0.0; featureCounts -O -M -T 32 -p -s 2). Differential gene testing was performed on counts normalized to library sizes scaled to external S2 spike-ins and filtered for lowly expressed genes using edgeR (v3.32.1) on Rstudio (v4.0.2). Gene Ontology analysis was performed using the ToppGene suite (63–65).

3′UTR-seq analysis

Single-end reads were demultiplexed using bcl2fastq (v2.17.1.14) and resulting FASTQ files were quality checked using fastqc (v0.11.6), trimmed 12 bp from the 5′ end to remove primer bias, trimmed for polyA stretches, and filtered for quality and length using cutadapt (v2.1; -u 12 -q 10 -m 20 -a AAAAAAAAAA). Trimmed reads were mapped to GRCh37/hg19 and BDGP R5/dm3 genomes using hisat2 (v2.1.0) using standard single-end settings and resulting SAM files were converted to BAM files using samtools (v1.9; view), which were then sorted (sort) and indexed (index). Reads mapping to exonic genomic intervals were counted using a hg19 GTF file and dm3 SAF file with FeatureCounts from the subread package (v2.0.0; featureCounts -O -M -F GTF -T 16 -s 0). Differential gene testing was performed on counts normalized to library sizes scaled to external S2 spike-ins and filtered for lowly expressed genes using edgeR (v3.32.1) on Rstudio (v4.0.2). The Broad Institute GSEA software was used to perform GSEA (62).

MAC-seq analysis

Paired-end reads were demultiplexed using bcl2fastq (v2.17.1.14) and resulting FASTQ files were quality checked using fastqc (v0.11.6) and read 2 (R2) was trimmed 15 bp from the 5′ end to remove primer bias using cutadapt (v2.1; -u 15). R2 FASTQ files of paired-end reads were demultiplexed according to well barcodes (Supplementary Table S9) and filtered for PCR duplicates using Unique Molecular Identifiers (UMIs), both present in read 1 (R1) using the scruff (66) R (v4.0.2) package dumultiplex function (bcStart = 1, bcStop = 10, bcEdit = 0, umiStart = 11, umiStop = 20, keep = 35, minQual = 20, yieldReads = 1e + 06). R2 FASTQ files were then mapped to the GRCh37/hg19 genome and ERCC sequences using alignRsubread (unique = FALSE, nBestLocations = 1, format = 'BAM') and resulting BAM files were used to count unique R2 reads mapping to exonic genomic intervals and ERCC sequences using a combined hg19/ERCC GTF file with countUMI (umiEdit = 0, format = 'BAM', cellPerWell = 1. Both functions are from the scruff R package. Gene expression counts were normalized to library size and reads mapping to ERCC spike-ins using the RUVseq R package (v1.24.1). Subsequent count processing was performed using the Seurat R package (v3.2.1) (67), where lowly expressed genes were filtered and counts were normalized for latent variables including plate, well row and column, using

the SCTransform function. SCTransformed scaled gene RNA expression values were then used for PCA, where shared-nearest-neighbours (SNN) network was calculated using the top 10 Principal Components with the FindNeighbours function using default parameters. Drug-treatment clusters were subsequently identified with the Louvain algorithm using a resolution parameter of 2. Uniform Manifold Approximation and Projection (UMAP) values were also calculated using the top 10 Principal Components with the RunUMAP function using default parameters. Differential gene testing relative to treatment controls (DMSO or EtOH) was performed using a hurdle model (MAST) with un-scaled gene RNA expression counts, plate and column numbers as latent variables and a logFC threshold of 0 with the FindMarkers Function. Area Under the Curve (AUC) scores for each drug treatment and gene lists indicated was calculated using all expressed genes with the R AUCell Package (v0.10.0).

ChIP-seq analysis and super-enhancer identification

H3K27ac ChIP-seq FASTQ files (SRR1957037, SRR1957038, GEO Accession GSM1652918) were downloaded using sratoolkit (v2.9.0, fastq-dump –gzip –split-files), quality checked using fastqc (v0.11.6) and mapped to the GRCh37/hg19 genome using bowtie2 (v2.3.4.1) with paired end read settings. Resulting SAM files were converted to BAM files using samtools (v1.9; view), which were then sorted and indexed. Potential PCR duplicates were filtered using the MarkDuplicates function from picard (v2.6.0; REMOVE_DUPLICATES = true) and BAM files were converted to TDF files using igvtools (v2.3.95; count -z 5 -w 10). H3K27ac peaks were called relative to input using macs (v2.1.1; callpeak -f BAMPE -g hs -q 0.01 -call-summits –cutoff-analysis) and peaks within hg19 ENCODE blacklist regions (https://www.encodeproject.org/files/ENCFF356LFX/) were removed using bedtools (v2.27.1) intersect function. Super-enhancer calling was performed using Ranking Ordering of Super-Enhancer (ROSE2) (v1.0.5; -c INPUT -g hg19 -t 2000 -s 12500) (68) and were annotated to genes according to 'TOP GENE.'

Genome-wide CRISPR Cas9 screening analysis

Trimmed 20 base pair reads from survival screens performed in THP-1 and MV4;11 Cas9 cells transduced with the Brunello genome-wide sgRNA library and cultured in either DMSO or AZ-5576 (CDK9i; 150nM) for 21 days from (69), were used for sgRNA counting with the MAGeCK algorithm, where read counts from treatment replicates were pooled (v0.5.6; mageck count). The MAGeCK algorithm test subcommand (mageck test) was then used to determine genes negatively selected in CDK9i relative to DMSO treatment groups. Visualization of screen data was performed in R (v4.0.2) using ggplot2 (v3.1.1) and ggrepel (v0.8.1) packages. Annotated RBPs were identified using data from (*70*).

Coltron analysis

The coltron algorithm (v1.0.2) (*27*) was used to identify SE-associated TFs and regulatory networks using ROSE2-determined super-enhancer peaks and H3K27ac BAM signal with default parameters.

TCGA survival analysis

SEM (RNA-Seq by Expectation Maximization) (*71*) scaled expression values (transcripts per million) for TCGA tumour samples were downloaded from the GDAC Firehose website. Entrez gene IDs were mapped to HGNC gene symbols using the biomaRt R package (version 2.42.0) and collapsed to unique values per gene symbol by selecting the most variable entrez ID among all samples for each gene symbol. Primary samples from the TCGA LAML cohort were selected using the TCGA biolinks R package (version 2.14.0) and were matched with overall survival (OS) endpoints from the TCGA Pan-Cancer Clinical Data Resource. Gene signature scores were calculated using the singscore R package,then used to fit Kaplan-Meier and Cox regression models to the OS endpoints using the survival R package (version 3.1–8).

Determination of RNA synthesis and decay rates

Solving the first order differential equation in $M(t) = k_1 - k_2 M(t)$ yields an exponential function with parameters for the synthesis rate (k_1), decay rate (k_2) and initial quantity of RNA (M_0):

$$M(t) = (M_0 - K)^* e^{\wedge}(-k_2{}^*t) + K$$

where $K = k_1/k_2$ is the quantity at equilibrium.

To determine decay rates (k_2) for each gene, precision-weighted nonlinear regression was used to fit an exponential curve to the decreasing quantity of SLAM-seq labelled reads measured post-washout of 4sU.

Assuming no synthesis of labelled reads post-washout ($k_1 = 0$) leaves one parameter for the starting RNA concentration, which was set to the initial data point at $T = 0$, and one for the decay rate, which was fit using MINPACK's (v1.2–1) Levenberg-Marquardt implementation in R.

Precision weights for the fit were estimated using local regression. The standard deviation between technical replicates for a given mean expression level in the baseline SLAM-seq dataset was modelled with R's `loess` implementation, and then applied to calculate weights for the other samples during fitting. Decay rates in hours are listed in Supplementary Table S10.

Synthesis rates were determined by dividing the TT-seq adjusted reads per million for each gene by the length and sampling time, producing a scaled FPKM h^{-1} averaged across replicates.

Predictions

Predictions were made with the model using the fitted rates and differing initial conditions, then compared against a separate dataset of total mRNA measurements at T = 2, 6 h.

Parameters set for simulated results:

Simulated Result	Decay rate (k_1)	Synth. rate (k_2)	Initial qty (M_0)
Simulated total transcriptional shutdown	Fitted decay rate under drug	0	Baseline equilibrium

Results

Broad scale nascent RNA changes in response to transcriptional perturbation are poorly reflected on the total mRNA level

To investigate the therapeutic response to agents that target proteins and complexes that regulate chromatin (22), the biological effect to small molecule inhibitors of p300/CBP (A-485), BRD4 (JQ1), CDK9 (AZ-5576) and RNAPII (actinomycin-D; ACTD) in the K562 chronic myeloid leukaemia (CML) cell line was assessed (Figure 1A and Supplementary Figure S1). All drug treatments resulted in reduced number of K562 cells grown *in vitro* with concentration- and time-dependent inhibitory effects (Supplementary Figure S1A). The small molecule concentrations used to assess the anti-leukaemic effects resulted in on-target inhibitory activities, as demonstrated by a reduction in H3K18ac, c-MYC protein and RNAPII carboxy-terminal domain (CTD) Serine 2 (Ser2) phosphorylation following treatment with A-485, JQ1 and AZ-5576/ActD, respectively (Supplementary Figure S1. B) (18,30,31).

To evaluate the transcriptional response to on-target doses of each inhibitor we performed thiol (SH)-linked alkylation for the metabolic sequencing of RNA (SLAM-seq) after 2 h of drug treatment (29) (Figure 1A, B). This conversion-based approach uses 4sU-dependent thymine-to-cytosine (T > C) conversions for the *in silico* separation of newly synthesized and pre-existing transcripts and enables direct quantification of both nascent and total mRNA levels (29). Differential gene expression analysis (DGEA) of the total mRNA read counts for drug-treated samples revealed that, for all inhibitors, only a subset of expressed genes showed changes in total mRNA levels (Figure 1C, Supplementary Figure S2A). To assess whether features such as SEs correlate with transcriptional responses observed, we defined SE and core regulatory CR-TF networks in K562 cells using H3K27ac signal (Supplementary Figure S2B) and the Coltron algorithm (32) (Supplementary Figure S2C, D), respectively. This revealed that SE-associated and CR-TF networks were significantly more down-regulated compared to all other genes across all treatments (Figure 1D, Supplementary Figure S2E, F). Similarly, transcripts encoding genes involved in cancer hallmark pathways such as c-MYC targets and cytokine signalling, were repressed with all inhibitors (Supplementary Figure S2G). This observation is consistent with the notion that chromatin features are predictive of the transcriptional response. Nonetheless, many of the SE-associated genes and CR-TFs were refractory to changes in total mRNA levels at the timepoints and inhibitor concentrations tested (Figure 1C, Supplementary Figure S2E, F), suggesting that other parameters determine the mRNA response to transcriptional inhibitors.

To assess the selectivity and specificity of the transcriptional response to these inhibitors we next analysed the nascent transcriptome. In contrast to the selective effect observed for total mRNA levels (Figure 1C, Supplementary Figure S2A), DGEA performed on nascent mRNA read counts following small molecule inhibition of p300/CBP, BRD4, CDK9 and RNAPII for 2 h revealed a broad repression in mRNA synthesis in response to all inhibitors (Figure 1E, Supplementary Figure S3A–C). The greatest effect on nascent mRNA expression was measured following treatment with AZ-5576 and ACTD, which globally down-regulated the mRNA synthesis of >80% of genes (Figure 1E, Supplementary Figure S3A–C). In contrast, transcriptional inhibition with p300/CBPi and BRD4i was more selective and significantly reduced the mRNA synthesis of <50% of expressed genes (Figure 1E, Supplementary Figure S3A–C). Importantly, changes in nascent gene expression with p300/CBPi and BRD4i treatment was still significantly greater than to the corresponding total mRNA changes (Supplementary Figure S3C). In fact, comparison between nascent and total mRNA read counts across all drug treatments revealed only a modest Pearson's correlation coefficient (Supplementary Figure S3D). This disconnect can be observed for genes such as *HPRT1* that were the least responsive on the total mRNA level but had significantly down-regulated nascent gene expression (Figure 1F, Supplementary Figure S3E). In contrast, for genes such as *c-MYC*, nascent mRNA changes directly translated to a reduction in total mRNA levels (Figure 1F, Supplementary Figure S3F). These observations highlight two aspects of gene regulation in response to transcriptional inhibitors: (i) The chromatin landscape can be predictive of the response on the mRNA level, but (ii) whether a gene will or will not respond is inherently driven by additional factors, independent of the chromatin state. Conversely, the chromatin state may simply correlate with the other transcriptional or post-transcriptional parameters that mechanistically define the response of a particular transcript.

mRNA decay rates influence the response to transcriptional inhibitors

We reasoned that post-transcriptional mechanisms such as RNA decay can be the causal parameter that shapes the response to transcription inhibition. It is well established that steady-state mRNA transcript levels are determined by transcript decay rates, and that acute inflammatory or growth response signals are reliant on the induction of short-lived transcripts (33). To enable accurate assessment of production and decay kinetics we measured the two parameters independently using transient transcriptome (TT) -seq and time-course 4sU pulse-chase labelling with SLAM-seq (Figure 2A, B). TT-seq was used instead of SLAM-seq for estimation of RNA production rates due to TT-seq using shorter 4sU labelling time (5 or 15 min versus 1 h), which reduces the likelihood of transcript decay rates affecting the mRNA production rate measurements (34). For pulse-chase SLAM-seq experiments the cells were labelled with 4sU for 12 h, followed by sampling during a 12 h window post 4sU washout. The concentration of 4sU that was chosen retained cell viability (Supplementary Figure S4A) and proliferation (Supplementary Figure S4B) throughout the experiment. Subsequently, decay kinetics were then quantitatively determined by fitting exponential decay functions to normalized transcript levels measured over the time course described above, which enabled the generation of estimated mRNA half-life ($t_{1/2}$) parameters for 6580 genes (Supplementary Figure S4C), including short-lived genes such as *c-MYC* ($t_{1/2} = 1.3$ h) (Supplementary Figure S4D). The measurements we obtained were concordant with published decay measurements obtained in K562 cells with conversion-based protocols (Supplementary Figure S4E) (35,36).

Integration of the production and decay datasets revealed that CR-TFs have extremely short transcript half-lives, driving the rapid turnover of newly produced RNA, thereby necessitating the high production rates, as observed by TT-seq (Figure 2B, Supplementary Figure S4F). The set of the most highly produced genes with rapid decay parameters correlated with poorer acute myeloid leukaemia (AML) patient overall survival (Supplementary Figure S4G–J) indicating that

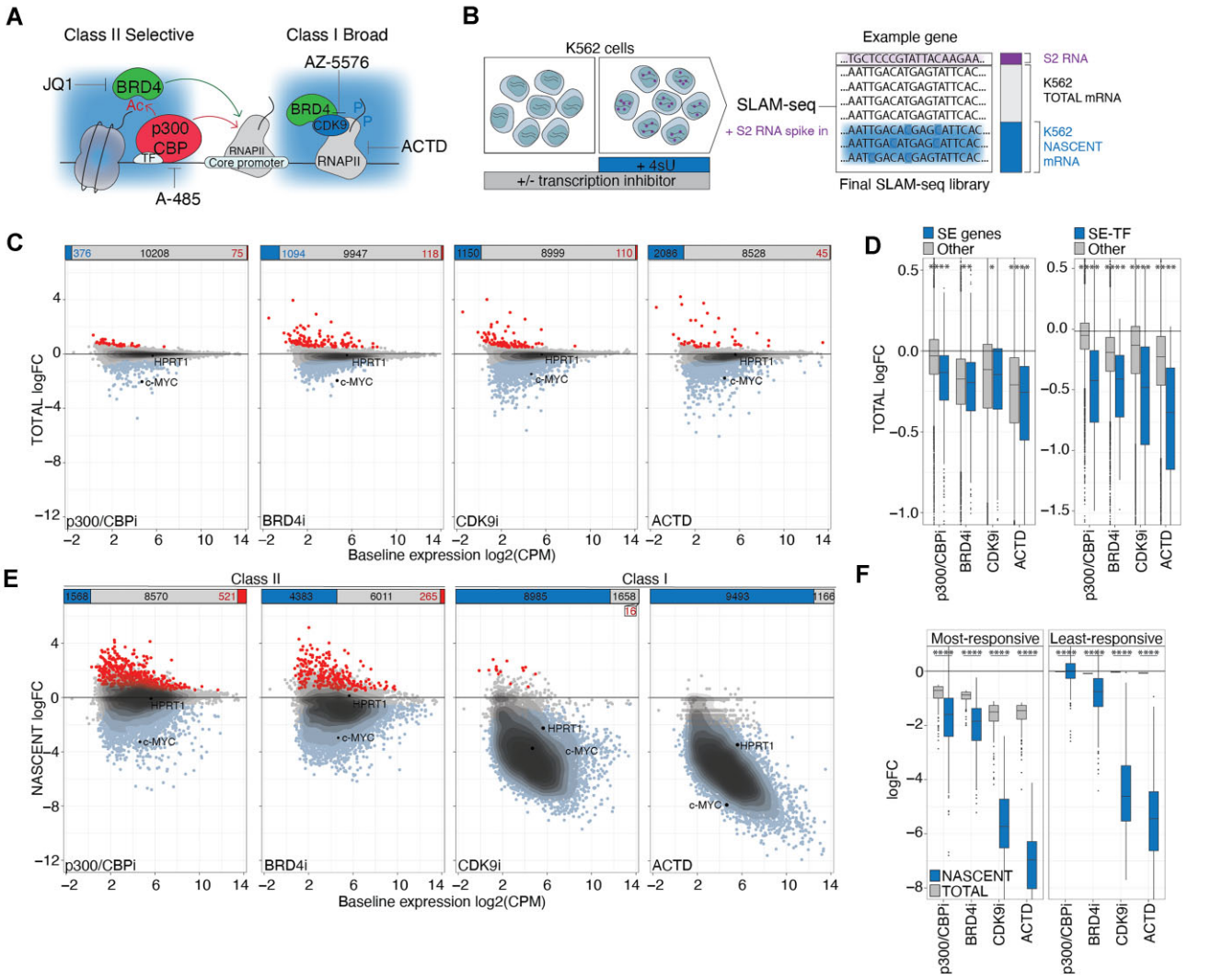

Figure 1. A defined subset of genes determines the therapeutic response to transcription inhibition. (**A**) Simplified schematic of transcription inhibition by A-485 (p300/CBPi), JQ1 (BRD4i), AZ-5576 (CDK9i) and Actinomycin-D (ACTD). (**B**) Schematic of SLAM-seq experimental procedure. Nascent reads are defined as RNA containing at least two thymine-to-cytosine (T > C) conversions and total reads are defined as the sum of unconverted and converted RNA. Schneider 2 (S2) RNA was spiked-in as an external reference control. Experiment was performed in technical duplicate. (**C**) Scatterplot of baseline total mRNA expression versus change in spike-in normalized total gene expression upon 2 h of transcription inhibition. Significantly up- or down-regulated genes highlighted in red and blue, respectively. Sum of significantly differentially altered events indicated in bar chart above. (**D**) Change in spike-in normalized total expression of (left) genes regulated by super-enhancers (SEs) and (right) core-regulatory transcription factors (CR-TF). Remaining genes indicated in grey. (**E**) Scatterplot of baseline nascent mRNA expression versus change in spike-in normalized total gene expression upon 2 h of transcription inhibition. Significantly up- or down-regulated genes highlighted in red and blue, respectively. Sum of significantly differentially altered events indicated in bar chart above. (**F**) Change in spike-in normalized total and nascent expression of (left) most- and (right) least-responsive genes. p300/CBP: p300/cAMP-response element binding protein (CBP). BRD4: bromodomain-containing protein 4. CDK9: cyclin dependent kinase 9. RNAPII: RNA polymerase II. TF: transcription factor. Ac: acetyl group. P: phosphate group. 4sU: 4-thiouridine. H: hour. 3′UTR: 3′ untranslated region. LogFC: $\log_2$ fold change relative to DMSO. Baseline expression: spike-in normalized total $\log_2$ CPM in DMSO-treated conditions. CPM: counts per million. Significantly up-regulated: *P* value < 0.05 & logFC > 0.5. Significantly down-regulated: *P* value < 0.05 & logFC < −0.5. *P* value < 0.0001 using an unpaired Wilcoxon test. Most-responsive: top 200 most significantly down-regulated genes (logFC < −0.5 and *P* Value < 0.05) using spike-in normalized total reads. Least-responsive: 200 unaltered (−0.25 < logFC < 0.25 and *P* Value > 0.05) genes using spike-in normalized total reads. AUC: area under the curve.

the isolated assessment of production and decay can define oncogenic networks that are clinically relevant for AML. Importantly, these observations could indicate that short transcript half-life is what drives the need for high production rates to sustain oncogenic transcript levels, thus exposing two distinct vulnerabilities to transcriptional perturbation; the requirement for rapid mRNA synthesis and inability to retain mRNA levels upon a transcriptional block (Figure 2B, Supplementary Figure S4F). We hypothesized that mRNA decay rates may in fact be the causative factor driving the selective changes in total mRNA levels upon transcription perturbation. Indeed, the most responsive genes to all inhibitors had half-lives approximately 3–4 times shorter than those least responsive to transcription inhibition, and the median half-life of each category varied little between different small molecule treatments (Figure 2C). The reversed analysis of grouping genes according to their transcript half-life and assessing their total mRNA levels was also consistent with short-lived

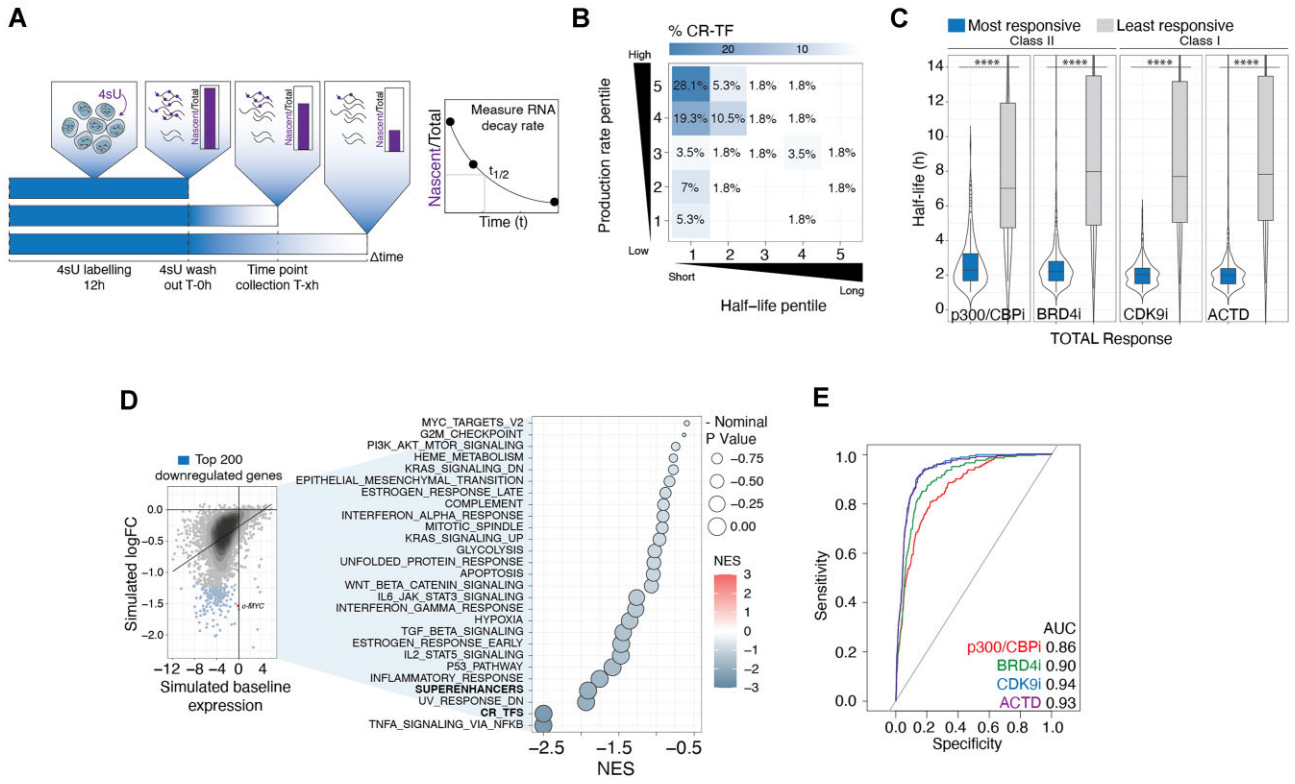

Figure 2. RNA decay rates influence the therapeutic response to transcriptional inhibitors. (**A**) Schematic of 4-thiouridine (4sU) pulse labelling and chase. T > C conversion rates were calculated for each time point, normalized to 0-h and fit with exponential decay functions derive half-life ($t_{1/2}$). Experiment was performed in technical duplicate. (**B**) Heatmap of percentage of CR-TFs present within each mRNA decay and production pentiles from Supplementary Figure S4F. (**C**) Boxplot of mRNA half-lives of genes most- and least-responsive to treatments indicated. (**D**) (Right) Simulation of total mRNA levels with complete transcription shutdown after 2 h and (left) associated GSEA analysis of hallmark, SE and CR-TF gene sets using ranked z-scored logFC values. Signatures with Normalized Enrichment Scores (NES) < 0 shown. (**E**) Receiver Operator Characteristic (ROC) analysis of total logFC with treatments indicated and simulated total logFC after complete transcription shutdown for 2 h. logFC values were binarized according to whether genes were most-responsive to treatments indicated. AUC: area under the curve. Most-responsive: top 200 most significantly down-regulated genes (logFC < −0.5 and *P* value < 0.05) using spike-in normalized reads. Least-responsive: 200 unaltered (−0.25 < logFC < 0.25 and *P* Value > 0.05) genes using spike-in normalized reads.

mRNAs being significantly down-regulated in comparison to longer-lived groups for all compounds tested (Supplementary Figure S5A) and enriched for genes defined as the most responsive (Supplementary Figure S5B). In contrast, genes that were least responsive to RNAPII-targeting were over-represented for longer $t_{1/2}$ gene categories (Supplementary Figure S5C). Although transcript half-life was the most predictive factor for total mRNA down-regulation for the most responsive genes, mRNA production rates also mattered in some contexts, with genes with the highest mRNA production rates and shortest half-lives being most strongly repressed following treatment with transcriptional inhibitors (Supplementary Figure S5D, E). These observations are not limited to the small molecule inhibitors chosen, as reanalysis of SLAM-seq datasets assessing c-MYC and BRD4 degradation or inhibition of BCR-ABL1 using nilotinib in K562 cells revealed that transcript half-life also defines the response to transcriptional disruption (19) (Supplementary Figure S6). Our model extended to THP-1 cells, with integration of decay parameters (this study) and transcriptional responses (previously published datasets (30)), demonstrating that RNA decay shapes the mRNA response (Supplementary Figure S7).

To quantitatively assess the impact of transcript half-lives on total mRNA abundance upon transcriptional inhibition, we developed a mono-exponential model of steady state gene expression using only mRNA production and decay rates (Supplementary Figure S8A). Production rates (k_1) and decay rates (k_2) were determined using the TT-seq and SLAM-seq measurements described above for K562 cells (Figure 2A). Predicted steady state mRNA levels significantly correlated with experimental measurements of baseline mRNA abundance (Supplementary Figure S8B), indicating that the model was sufficiently accurate to estimate equilibrium mRNA levels with a variety of initial conditions and time intervals. To predict the effects on total mRNA abundance following 2 h of transcription inhibition, akin to our SLAM-seq experiments with small molecules (Figure 1), we set the mRNA production rate of each gene to zero in our model (Supplementary Figure S8A, C). This means that any change in total mRNA is due to decay rate alone. In line with our biological data (Figure 1C, Supplementary Figure S2G), *in silico* transcripts encoding TFs, cytokine signalling, inflammatory and *c-MYC* target cancer hallmark pathways and SE-transcriptional programs, were amongst the most reduced in total RNA (Figure 2D, Supplementary Figure S8D, E). Consistently, simulated total RNA levels following transcription shutdown (Figure 2D, Supplementary Figure S8C, D) significantly correlated with experimental total mRNA measurements with each compound (Figure 1C), albeit most strikingly with CDK9i and ACTD (Supplementary Figure S8F). Indeed, transcripts

most down-regulated *in silico (*genes with the shortest mRNA $t_{1/2}$) predicted transcripts that were selectivity repressed on the total mRNA level regardless if class I or class II inhibitors were deployed. Predictive accuracy was higher with class I inhibitors (AUC 0.93–0.94) in comparison to class II (AUC 0.86–0.90) (Figure 2E). Importantly, small molecules used did not greatly affect transcript half lives, where modelling of complete transcriptional shutdown using treatment-specific mRNA decay rates (Supplementary Figure S9A–D) correlated significantly with experimentally measured total mRNA changes (Supplementary Figure S9E).

Taken together, these data highlight that changes in total mRNA with chromatin modifiers and transcriptional inhibitors is strongly determined by mRNA decay rates, particularly with class I inhibitors. However in the context of class II inhibitors, distinct total mRNA changes stem from combination of both selective inhibition of mRNA production and $t_{1/2}$. As such, these findings suggest that mRNA decay rates can define a distinct set of responsive genes with reduced total RNA levels upon transcriptional inhibition in a manner that is agnostic to the chromatin landscape or the molecular consequences of the cofactor targeted.

MAC-seq reveals the influence of mRNA decay rates to changes in gene expression

Thus far, we have demonstrated that RNA decay rates are important in determining total RNA responses to a subset of transcriptional inhibitors. To assess the role of mRNA half-lives to gene expression responses across a wider range of clinically relevant inhibitors, we used Multiplexed Analysis of Cells sequencing (MAC-seq) to profile total mRNA changes in response to 73 small molecule inhibitors targeting epigenetic and transcriptional proteins in K562 cells (Figure 1A, Supplementary Figure S10. A). All compounds were used at a concentration of 1μM for 6 h. DGEA revealed a number of differentially expressed events (Figure 3B), where 8 out of the 73 compounds tested globally repressed transcription and significantly down-regulated > 1000 genes (Figure 3C). This first group of inhibitors (termed class I) target cofactors described to exhibit broad gene specificities (22), including those able to perturb t-CDKs and the core RNAPII machinery (Pan-Tx) (Figure 3C, Supplementary Figure S10A). Moreover, a second group (class II) of an additional six agents targeting BRD4, p300/CBP, histone deacetylases (HDACs), and protein phosphatases (PP), were able to selectively down-regulate a subset of at least 200 genes (termed class II compounds), chromatin-dependent activities and in line with our previous observations (22) (Figure 3C, Supplementary Figure S10A). Remaining compounds, defined as class III, that targeted histone demethylases (HDMe) and methyltransferases (HMe), DNA alkyl- (DNA AGT) and methyl- transferases (DNAMe), sirituin (SIRT), PARP, ELAVL1/HuR and topoisomerases (Topo) either repressed the expression of a minimal number of genes (<200) or primarily up-regulated transcription (Figure 3C). This indicates that mRNA stability is less likely to influence the total transcriptome for class III compounds.

To characterize gene expression responses between compounds, uniform manifold approximation and projection (UMAP) of drug treatments was performed. This revealed that gene expression responses grouped according to drug treatment (Supplementary Figure S10B, middle), drug protein target (Supplementary Figure S10B, bottom) and family (Figure 3D, top) and class (Figure 3D, middle). Notably, despite all class I compounds forming an entirely distinct cluster (Figure 3D, middle), more detailed analysis of this drug class in an isolated setting revealed separation between Pan-Tx, CDK9/7/12/13 and CDK11/12/13 inhibitors (Figure 3D bottom, S10A). This suggests that though class I compounds can broadly repress gene expression, they are mechanistically distinct and not equivalent. Inhibitors within the class II category, except for drugs targeting BET proteins, also clustered separately (Figure 3D, bottom, Supplementary Figure S10A), highlighting that they induce distinct and selective transcriptional responses in line with previously defined chromatin specificities (22).

It was next assessed if our previously measured mRNA decay rates determine the gene expression responses to other compounds able to globally (class I) or selectively (class II) repress gene expression as defined by MAC-seq (Figure 3C). Genes most responsive to class I and II inhibitors were significantly shorter lived in comparison to genes least responsive to transcriptional targeting (Figure 3E, Supplementary Figure S10C). The difference in half-life between most and least responsive gene sets was most striking with class I inhibitors, where mRNA stability varied up to 3-fold between the two categories (Figure 3E, Supplementary Figure S10C). Consistently, grouping transcripts according to their half-life instead, as defined previously in Figure 2, revealed that short-lived mRNAs were enriched as mRNAs most responsive to transcriptional targeting by class I and II inhibitors (Figure 3F). This was more evident with class I compounds, which had >40% of most-responsive genes within the most short-lived group (Figure 3F). In agreement with these data, short-lived mRNAs were significantly depleted in response to class I compounds in comparison to class II and III mRNAs (Supplementary Figure S10E). Focusing on genes encoding the most long-lived mRNAs instead revealed that they were least-responsive to targeting by most inhibitors within the two classes (Supplementary Figure S10D) and consequently, were found to be significantly over-represented across mRNAs in responses to class I and II compounds compared to class III (Supplementary Figure S10F). Furthermore, transcripts with short half-lives were highly predictive as genes amenable to t-CDK and general RNAPII inhibition using models of complete transcription shutdown (Figure 3G), consistent with previous findings (Figure 2E). Due to selective targeting observed on the nascent mRNA level and longer drug incubation times required, predictive accuracy was modest with BRD4, p300/CBP, pan-HDAC and PP targeting (Figure 3G). Taken together, these data demonstrate that the role of mRNA decay can be extended to several transcriptional and epigenetic inhibitors, where both selective and global down-regulation of gene expression is strongly dictated by mRNA decay.

c-MYC mRNA stabilization does not rescue biological and transcriptional effects of transcriptional targeting

A putative common effector mechanism of transcription inhibitors in leukaemia is repression of *c-MYC* (24). In K562 cells, *c-MYC* is necessary for driving the expression of a conserved set of gene targets encoding proteins necessary for nucleotide biosynthesis (23). Having determined that *c-MYC* transcript itself is short lived (Supplementary Figure S4D), we sought to assess whether altered *c-MYC* transcript

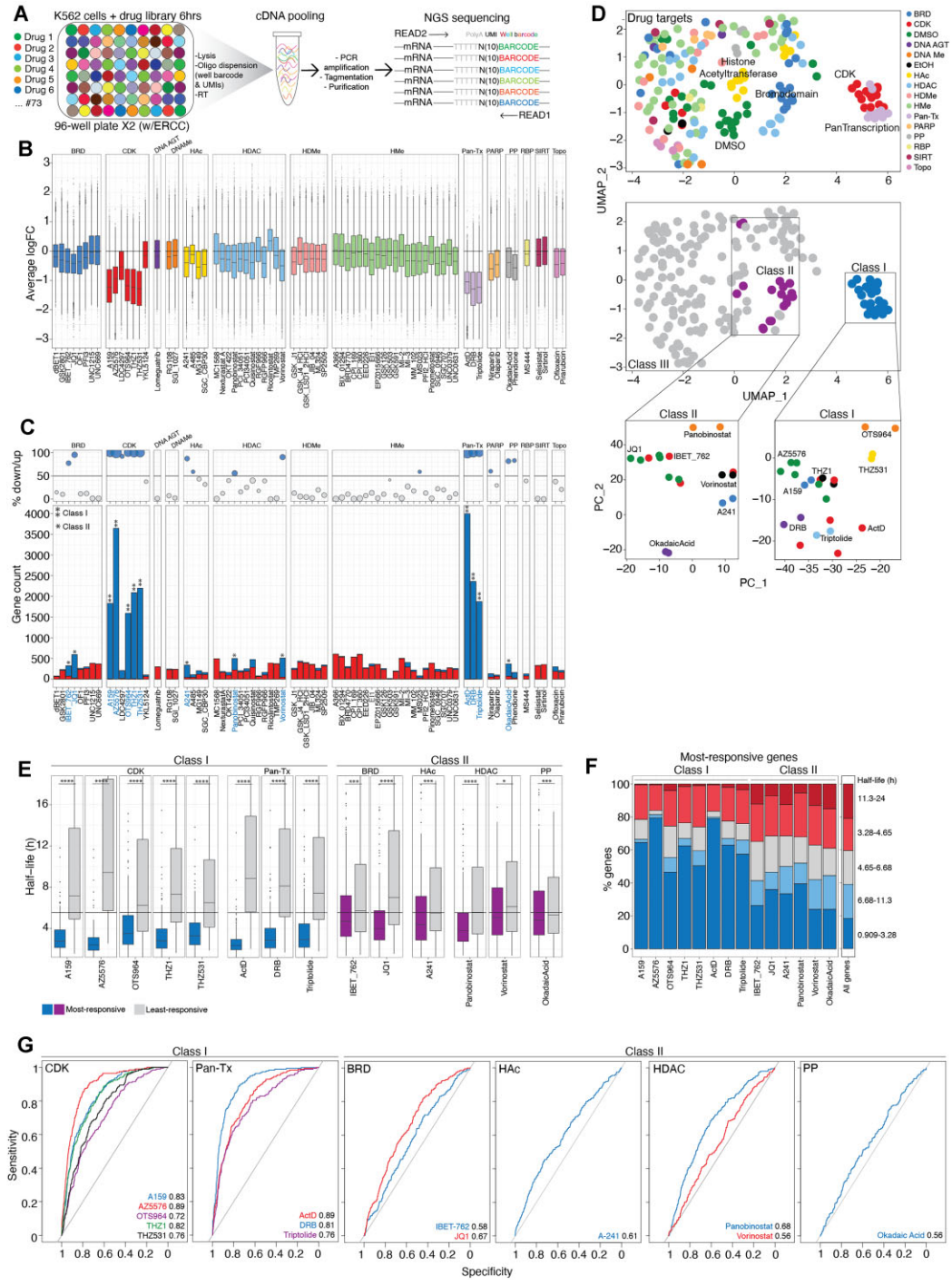

Figure 3. RNA decay rates influence the therapeutic response to several epigenetic and transcriptional inhibitors as defined by MAC-seq. (**A**) Schematic of MAC-seq experimental procedure. Experiment was performed in technical duplicate. (**B**) Box plot of change in gene expression relative to DMSO/EtOH controls with inhibitors indicated. Inhibitors are grouped according to drug protein target family. (**C**) (Top) Percentage ratio or (bottom) absolute number of significantly up- and down-regulated genes. Inhibitors able to significantly down-regulate >1000 genes are termed 'Class I' and by **. Inhibitors able to significantly down-regulate >200 genes are termed 'Class II' and indicated by *. Remaining compounds as designated as class III. (**D**) Uniform manifold approximation and projection (UMAP) of treatment conditions with (top) drug protein target family (middle) or pre-defined classes highlighted. (Bottom) PCA plot of drug classes (right) II and (left) I with drug names shown. (**E**) Boxplot of mRNA half-life of most- and least-responsive genes to class I and II inhibitors. (**F**) Bar chart representation of mRNA half-life pentiles in genes most-responsive to class I and II inhibitors. (**G**) Receiver Operator Characteristic (ROC) analysis of logFC with class I and II inhibitors and simulated total logFC after complete transcription shutdown for 6 h. logFC values were binarized according to whether genes were most-responsive to treatments indicated. UMI: unique molecular identifier. logFC: $\log_2$ fold change. BRD: bromodomain. CDK: cyclin-dependent kinase. DNA AGT: DNA alkyl-transferase. DNAMe: DNA methyl-transferase. HAc: histone acetylase. HDAC: histone deacetylase. HDMe: histone demethylase. HMe: histone methyl-transferase. Pan-Tx: Pan-transcription. PP: protein phosphotase. RBP: RNA binding protein. SIRT: sirtuin. Topo: topoisomerase. Significantly up-regulated: *P*-value < 0.05 and average logFC > 0.5. Significantly down-regulated: *P*-value < 0.05 and average logFC < −0.5. logFC: $\log_2$ fold change relative to DMSO/EtOH. AUC: area under the curve. Most-responsive: top 200 most significantly down-regulated genes (logFC < −0.5 and *P* value < 0.05) using spike-in normalized reads. Least-responsive: 200 unaltered (−0.25 < logFC < 0.25 and *P* value > 0.05) genes using spike-in normalized reads.

decay rates could modulate responses to transcriptional inhibition. As *c-MYC* stability is regulated by AU-rich elements (AREs), AUUUA and miRNA recognition motifs within its 3′UTR (37–40), CRISPR/Cas9-mediated homology directed repair (HDR) in K562 cells was used to substitute the *c-MYC* endogenous 3′UTR for the 3′ region of the longer-lived gene *HPRT1* together with a destabilized GFP (dsGFP) reporter, termed '*c-MYC-HPRT1* 3′UTR' (Figure 4A). Designated as '*c-MYC*-control 3′UTR', dsGFP was knocked-in 5′ of the endogenous *c-MYC* 3′UTR sequence as a control cell line (Figure 4A). Both cell models were validated by PCR (Supplementary Figure S11A–F) and Sanger sequencing (Supplementary Figure S11G, H). As our system genetically engineered the endogenous 3′UTR of *c-MYC*, its genomic location, in addition to *cis*- and *trans*-factors that impact its regulation, remained unaffected. Assessment of mRNA stabilities demonstrated that knock-in of the *HPRT1* 3′UTR increased the half-life of the chimeric *c-MYC* transcript by approximately 8 h following treatment with Actinomycin D (ACTD), representing a 4-fold increase over the half-life of the endogenous and entopic control *c-MYC* transcripts (Figure 4B, Supplementary Figure S12A, B). Moreover, *c-MYC* transcript stabilization did not alter baseline *c-MYC* total mRNA abundance (Supplementary Figure S12C), in contrast to nascent mRNA levels, where it was significantly lower in comparison to the control (Supplementary Figure S12D). Lower nascent *c-MYC* mRNA upon increased mRNA stability may have arisen from 'transcript buffering' or clonal cell differences.

To further investigate the response of stabilized *c-MYC* to RNAPII targeting, c-*MYC*-control and *c-MYC-HPRT1* 3′UTR cell lines were treated with 1 μM of the class I compounds AZ-5576 (CDK9i) or ACTD for 6 h and whole transcriptome RNA-Seq was performed. Consistent with previous findings (Figures 1, 3), DGEA of exon and intron reads revealed a global decrease in total and nascent gene expression respectively (Supplementary Figure S12E–G). Whilst *c-MYC* mRNA synthesis was significantly down-regulated irrespective of *c-MYC* mRNA half-life as assessed by *c-MYC* intron expression (Figure 4C, right), assessment of *c-MYC-dsGFP* total mRNA (Figure 4C, left*)* and protein abundance (Figure 4D, Supplementary Figure S12H–K) revealed that *c-MYC* stabilization rendered it less sensitive to targeting by either AZ-5576 (CDK9i) or ACTD. The resistance to RNAPII targeting on the total mRNA level was *c-MYC* specific, as *c-MYC* was the most significantly altered gene with each treatment (Figure 4E) and clustering of total mRNA changes highlighted that samples still grouped according to the inhibitor used and not cell line (Supplementary Figure S12L). Consistently, correlation analysis of all DEGs in c-*MYC*-control and -*HPRT1* 3′UTR cell lines with CDK9i and ACTD revealed that changes were highly similar and significant (Pearson's correlation coefficient 0.96–0.97, *P*-value < 2.2e-16) (Supplementary Figure S12M). As mentioned above, increasing *c-MYC* mRNA half-life through swapping of the endogenous *c-MYC* 3′UTR with that of *HPRT1* only rescued *c-MYC* mRNA levels and did not rescue the expression of previously defined *c-MYC* target genes (Supplementary Figure S12N, O) (11). Although nascent *c-MYC* target gene expression was significantly less down-regulated with CDK9i treatment in the c-*MYC-HPRT1* 3′UTR cell line (Supplementary Figure S12N), it was not sufficient to prevent reductions in mRNA levels of *c-MYC* targets (Supplementary Figure S12N). In line with these data, the proliferation and survival between K562 c-*MYC*-control and -*HPRT1* 3′UTR cell lines was not altered upon CDK9i and ACTD treatment *in vitro* (Figure 4F).

Taken together, these data suggest that class I inhibitors can mediate anti-leukemic effects even when expression of a key target gene, *c-MYC*, is maintained due to prolonged mRNA half-life. This challenges the notion that loss of *c-MYC* expression is necessary for the biological and molecular consequences of perturbing mRNA synthesis using agents such as AZ-5576 or ACTD. mRNA decay rates are thus a key determinant in establishing gene responsiveness, such as that of *c-MYC* and indeed many MYC-regulated genes, to compounds that target RNAPII driven gene expression, and without which, selective responses would not be found with most transcriptional compounds.

Selective modulation of mRNA decay through ELAVL1 targeting in THP-1 cells

Having established that the therapeutic response to transcriptional inhibition is shaped by mRNA decay rates, we next investigated whether mRNAs with long half-lives and consequently, not amenable to perturbation, could be sensitized to RNAPII targeting in leukaemia. We therefore reanalysed our previously published genome-wide CRISPR-Cas9 knockout screening datasets performed in AML cell lines treated with CDK9i, with a focus on RBPs due to their ability to bind mRNAs at specific sequence motifs to affect mRNA post-transcriptional processing (5). The analysis revealed that knockout of 16 RBPs sensitized both THP-1 and MV4;11 AML cell lines to CDK9i (Figure 5A, Supplementary Figure S13A). This included the RBP ELAVL1 (Figure 5A, Supplementary Figure S13A, B), which has been reported to stabilize oncogenic transcripts in AML and promote leukemic stem cell (LSC) self-renewal and survival (14,41). Importantly, ELAVL1 is the only pharmacologically targetable RBP target identified in our screen and was therefore selected for further functional analysis. To independently validate the results from the genome-wide screens, THP-1 cells with Cas9-mediated knockout of *ELAVL1* (Figure 5B) were demonstrated to be sensitized to the anti-leukemic effects of AZ-5576 after 72 h of treatment as determined using both competition and IC50 assays (Figure 5C, D, Supplementary Figure S13C). Given the proposed oncogenic role of *ELAVL1* (14,41), it was unsurprising to observe that *ELAVL1* knockout also resulted in a proliferative disadvantage in the absence of any CDK9i treatment (Figure 5D). This was concomitant with a modest decrease in global total mRNA levels (Supplementary Figure S13D, E) and an enrichment of interferon signalling pathways (Supplementary Figure S13F), in line with previous reports in THP-1 cells and validating our experimental model (39).

To interrogate the mechanism of CDK9i sensitization mediated by ELAVL1 knockout, THP1 cells expressing wild-type *ELAVL1* and with Cas9-mediated *ELAVL1* deletion were treated with CDK9i for 6 h and 3′UTR RNA-seq was performed. Consistent with our findings (Figures 1, 3), DGEA of total read counts revealed a global decrease in total gene expression with CDK9i across both *ELAVL1* wild-type and knockout cell lines, where the magnitude of global transcript down-regulation was modestly greater in ELAVL1 knockout cells (Figure 5E, Supplementary Figure S13D, G). Whilst the CDK9i response between cell lines was similar, as demonstrated by co-clustering of samples (Supplementary Figure S13H) and correlation analysis (Pearson's correlation coef-

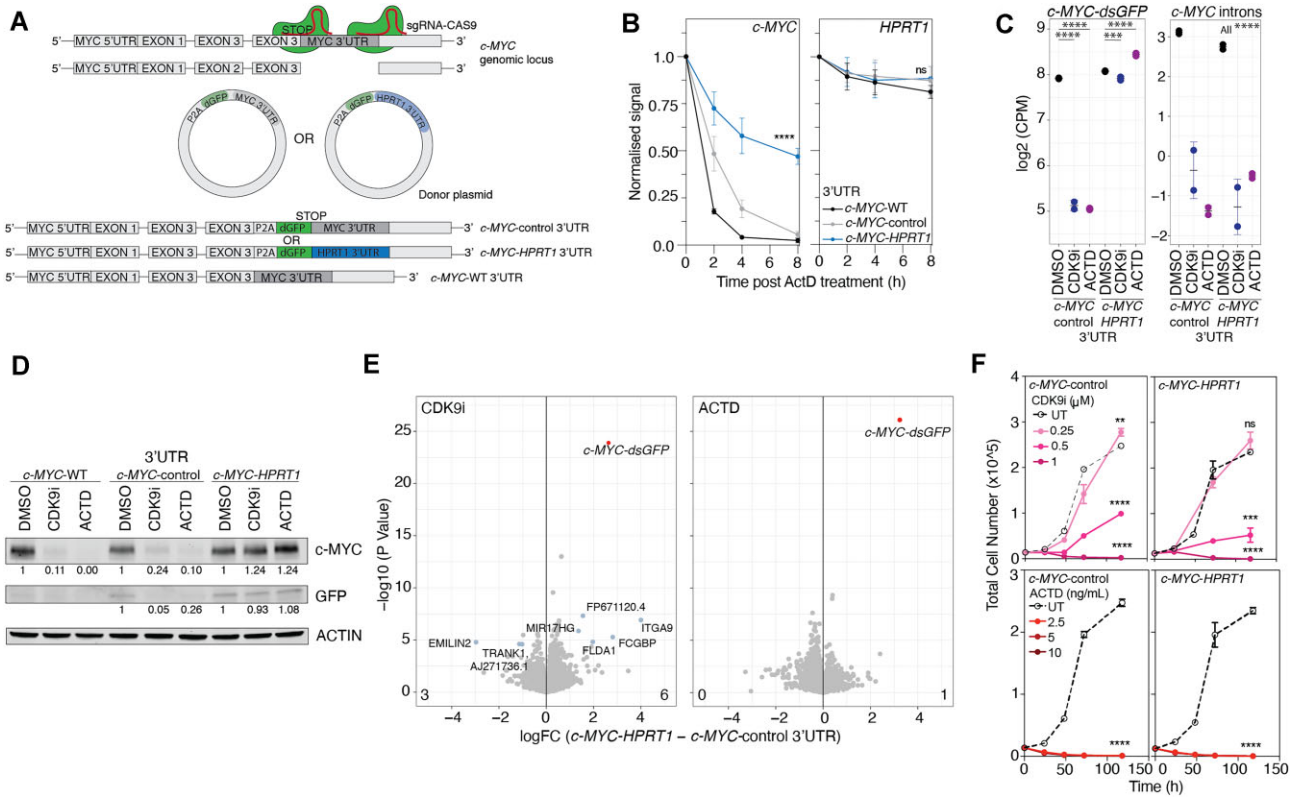

Figure 4. Increased *c-MYC* RNA stability does not rescue biological and transcriptional effects of transcriptional inhibitors. (**A**) Schematic of CRISPR/Cas9 -homology directed repair (HDR) used to endogenously swap the *c-MYC* 3′ untranslated region (3′UTR) for the *HPRT1* 3′UTR in the K562 cell line. (**B**) Normalized expression of (left) *c-MYC* and (right) *HPRT1* transcripts following the addition of ACTD at indicated time points as measured by quantitative real time PCR (qRT-PCR). Values are mean with error bars representing standard deviation (sd) of three biological replicates from three separate single cell clones. Data was analysed using a two-way ANOVA. **** and ns : *P*-value < 0.0001 and not significant, respectively. (**C**) (Left) Total gene expression of reads mapping across *c-MYC* and *dsGFP* sequences with indicated treatments and cell lines after 6 h. (Right) *c-MYC* intron expression with indicated treatments and cell lines after 6 h. Experiment was performed in technical duplicate. Data was analysed using edgeR. **** and ***: adjusted *P*-value < 0.0001 and 0.001, respectively. (**D**) Western blot of (top) c-MYC, (middle) GFP and (bottom) ACTIN protein with indicated treatments and cell lines after 6 h. Values indicated are protein levels normalized to ACTIN and DMSO controls. Image is representative of three biological replicates. Summary data is indicated in Supplementary Figure S12H. (**E**) Scatter plot of significance and difference in total gene expression with (left) CDK9i and (right) ACTD treatment between *c-MYC*-control and *-HPRT1* 3′UTR cell lines. (**F**) Total cell number over time of indicated cell lines treated with increasing concentrations of (top) CDK9i and (bottom) ACTD. Values are mean with error bars representing standard deviation (sd) of three biological replicates. Data was analysed using a two-way ANOVA. ****, ***, ** and ns : *P*-Value < 0.0001, 0.001, 0.01 and not significant, respectively. logFC: $\log_2$ fold change.

ficient 0.917, *P*-value < 2.2e-16) (Supplementary Figure S13I), further investigation revealed 57 genes that were significantly more down-regulated (logFC < −1 and adjusted *P* value < 0.01) upon ELAVL1 genetic depletion (Figure 5E, Supplementary Figure S13. J). As ELAVL1 has been described to regulate mRNA stabilities, the half-lives of the 57 transcripts sensitized to CDK9i following *ELAVL1* knockout were assessed. Using previous transcript decay measurements in THP-1 cells (Supplementary Figure S7G), it was evident that whilst the 20% most short-lived mRNAs were enriched in transcripts sensitized in *ELAVL1* knockout upon CDK9i, there was a subset of transcripts with longer half-lives (Figure 5F, left). Moreover, incorporation of THP-1 dependency scores obtained from the Broad Institute Depmap Portal demonstrated that sensitized transcripts with longer half-lives were highly essential, such as *NIFK* and *MED29* (Figure 5F, right, G). Indeed, both *NIFK* and *MED29* have been associated with oncogenic characteristics in a variety of cancer types (40,41). Collectively, our findings highlight that leukaemia cell line sensitization to CDK9i following *ELAVL1* knockout may be associated with the perturbation of essential mRNAs with long half-lives, which would otherwise be less amenable to transcriptional perturbation in *ELAVL1* wild-type cells.

To assess whether ELAVL1 knockout phenotypes observed in THP-1 cells (Figure 5A–D) could be rescued by ELAVL1 over-expression, we expressed sgRNA-resistant ELAVL1 in THP-1 cells that also express Cas9 and doxycycline-inducible control or ELAVL1 sgRNAs previously used (Figure 5B). To validate this model system, ELAVL1 sgRNAs were induced with doxycycline for four days and ELAVL1 exogenous and endogenous protein levels were assessed (Supplementary Figure S14A). Whilst exogenous ELAVL1 was less expressed in ELAVL1 knockout in comparison to wild-type backgrounds, ELAVL1 sgRNAs were able to reduce endogenous but not exogenous ELAVL1 levels (Supplementary Figure S14A). These data therefore validate the use of this model system for rescue experiments. To assess whether expression of exogenous ELAVL1 could de-sensitize cells to CDK9i, we performed competition assays in the presence of DMSO or AZ-5576 as previously described (Figure 5C). Counterintuitively, overexpression of ELAVL1 in the wild-type background resulted in slowed growth and further sensitized cells to CDK9i

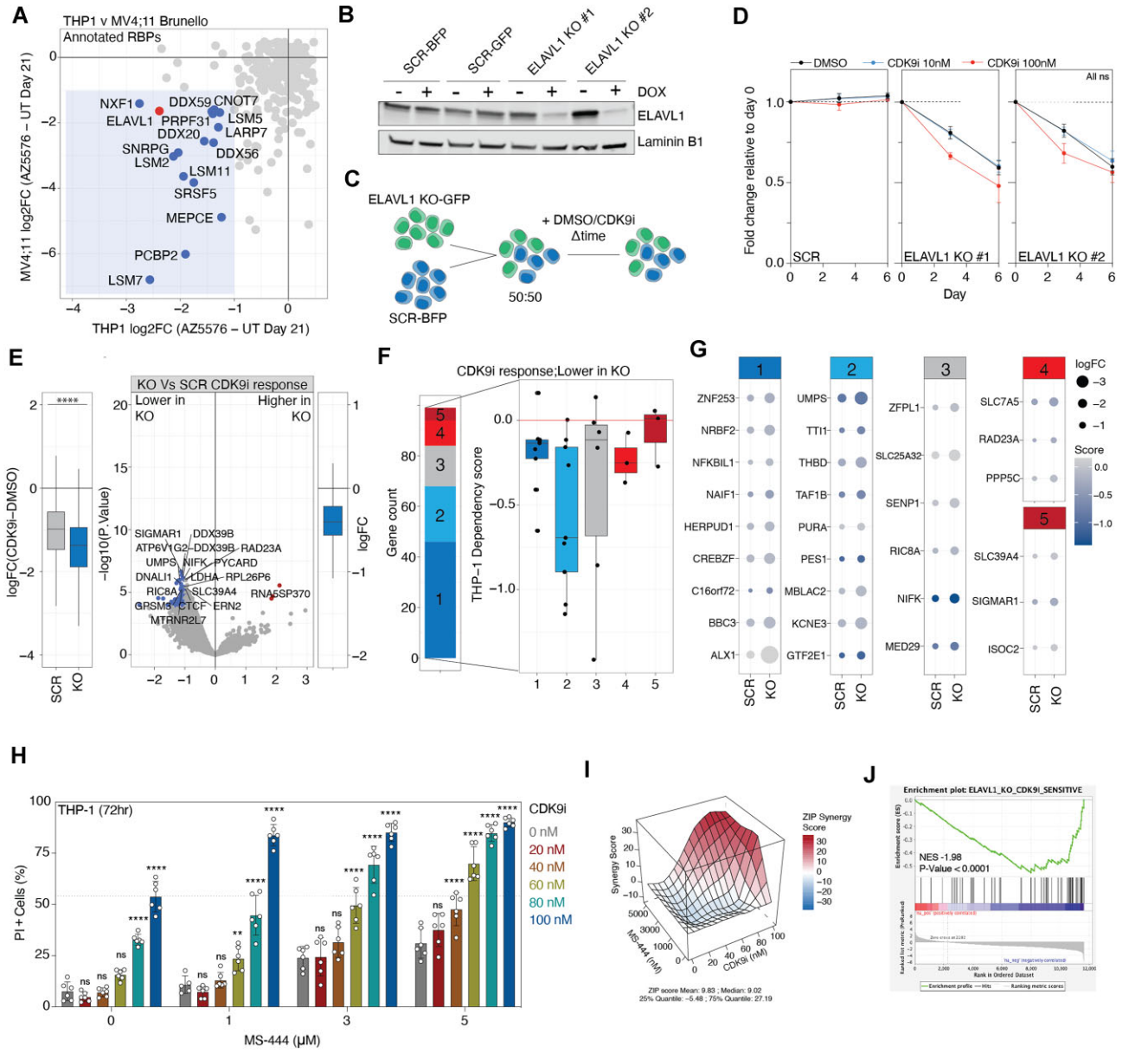

Figure 5. Dual targeting of CDK9 and ELAVL1 is synergistic in the THP-1 AML cell line. (**A**) Scatter plot of change in sgRNA read counts in CDK9i compared to untreated (UT) CRISPR-Cas9 genome-wide screening groups after 21 days of passaging in THP-1 and MV4;11 AML cell lines. Annotated RBPs that are down-regulated (logFC <−1) in both THP-1 and MV;11 cell lines indicated in blue and red (ELAVL1). Data is obtained from (*72*). (**B**) Western blot of (top) ELAVL1 and (bottom) Laminin B1 protein with indicated treatments and THP-1 cell lines after four days. Image is representative of three biological replicates. (**C**) Simplified schematic of competition assay experimental design. THP-1 cells expressing Cas9 and non-targeting control sgRNA (SCR) and sgRNAs targeting ELAVL1 (ELAVL1 knockout) are mixed in a 1:1 ratio and passaged in the presence of DMSO or CDK9i. (**D**) Fold change relative to day 0 of THP1 ELAVL1 knockout cells in competition with SCR cells as described in (C) at time points and treatments indicated. Values are mean with error bars representing standard deviation (sd) of three biological replicates. Data was analysed using a two-way ANOVA. Ns: *P*-value not significant. (**E**) (Left) Boxplot of spike-in normalized total mRNA reads with CDK9i relative to DMSO in THP-1 SCR and ELAVL1 KO cells. (Right) Scatter plot of significance and difference in spike-in normalized total gene expression of CDK9i response in ELAVL1 knockout relative to SCR cells. Significantly down- and up-regulated genes are highlighted in blue and red, respectively. (**F**) (Left) Stacked bar chart of previously determined transcript half-life pentiles in THP-1 cells across mRNAs sensitized to CDK9i upon ELAVL1 knockout (lower in KO; logFC < −1 and adjusted *P* Value < 0.01) and (Right) associated boxplot and (**G**) dot plot of THP-1 gene dependency scores from the Broad Institute Cancer Dependancy Map. LogFC values in each cell line are indicated. (**H**) Bar plot of THP-1 cell death (propidium iodide (PI) positive) in response to CDK9i and MS-444 at concentrations indicated following 72 h. Values are mean with error bars representing standard deviation (sd) of two biological replicates in technical triplicate. Data was analysed using a two-way ANOVA. **** and **: *P*-Value < 0.0001 and 0.01, respectively. (**I**) ZIP synergy scores derived from (H). Representative of first replicate. (**J**) Gene set enrichment analysis (GSEA) of genes significantly down-regulated with CDK9i in ELAVL1 knockout cells ranked using MS444 and CDK9i versus CDK9i RNA-seq data. NES: normalized enrichment score.

(Supplementary Figure S14B). This phenotype was similarly observed in the ELAVL1 KO #1 cell line (Supplementary Figure S14B). In contrast, the ELAVL1 KO #2 cell line was able to be rescued and de-sensitized to CDK9i with exogenous ELAVL1 expression (Supplementary Figure S14B). Though these data suggest that exogenous ELAVL1 may potentially rescue phenotypes observed with CDK9 targeting, the disparate results across the ELAVL1 knockout background cell lines makes this challenging to conclude.

To interrogate the therapeutic potential of ELAVL1 targeting in the context of CDK9i in leukaemia, THP-1 cells were treated with CDK9i in combination with the small molecule MS-444, an inhibitor of ELAVL1 (42). Importantly, MS-444 has been demonstrated to exhibit single agent efficacy in models of leukaemia *in vivo* (14). Assessment of cell viability using two experimental approaches revealed that the drug combination resulted in greater cytotoxicity than each inhibitor alone and displayed a level of synergy (Figure 5H, I, Supplementary Figure S15A–C). To next evaluate if this synergy was the result of the sensitization of longer-lived mRNAs to transcriptional targeting by CDK9i, THP-1 cells were treated with CDK9i and/or MS-444 for 6 h followed by 3′RNA sequencing. DGEA revealed that MS-444 alone did not markedly affect gene expression changes (Supplementary Figure S15D), in line with our genetic experiments (Supplementary Figure S13E). Comparisons of gene expression changes between MS-444 treatment and ELAVL1 knockout demonstrated poor correlation (Supplementary Figure S15. E). Discordance between drug and genetic data may be potentially derived from different ELAVL1 targeting times. Alternatively, targeting RNA decay in the presence of ongoing transcription is difficult to measure and may also explain the disparity observed. Indeed, further analysis showed that MS-444 in combination with CDK9i further down-regulated gene expression in comparison to either agent alone (Supplementary Figure S15E, F) and that this significantly correlated with ELAVL1 KO cell lines treated with CDK9i (Supplementary Figure S15G). Importantly, transcripts down-regulated in the drug combination were also enriched for genes repressed in ELAVL1 KO cell lines treated with CDK9i (Figure 5J) and included example mRNAs such as NIFK, MED29, SIGMAR1 (Supplementary Figure S15H). Taken together, these data are in line with our genetic ELAVL1 knockout experiments and suggest that the therapeutic perturbation of the mRNA decay and transcriptional machinery through pharmacological inhibition of ELAVL1 is an actionable and novel combination therapy for the treatment of AML.

Discussion

RNAPII-driven transcription has been pharmacologically targeted across solid and haematological malignancies with biological and therapeutic effects proposed to occur through selective perturbation of oncogenic gene networks (1,43). The current literature suggests that the selective targeting of genes following transcriptional perturbation is mechanistically linked to association with enhancers, SEs and disproportionate occupancy of critical chromatin co-factors, such as BRD4 and TFs, at promotors; however, the role of mRNA stability has not been extensively assessed in this context. Whilst selective responses upon transcription inhibition exist, their impact is far more wide-spread and less selective when assessed at the nascent RNA level. Critically, mRNA decay rates impose a critical filter between the nascent and total mRNA response resulting in selective responses even when they are not apparent at the nascent level. This means that selective transcriptional responses observed at the mRNA level can simply result from differences in mRNA decay rates and hint that, at least in the therapeutic context, selectivity at the gene-level is overestimated. This does raise the question why transcriptional networks in cancer may be more dependent on short-lived transcripts and therefore core-transcriptional components.

Here, we demonstrate that direct and indirect perturbation of RNAPII-driven transcription by class I and II therapeutic inhibitors respectively results in discrete alterations in total mRNA abundance that are defined by transcript decay rates (Figure 6). Both class I and II inhibitors reduce the total mRNA levels of genes with highly produced and short-lived transcripts, several of which are CR TFs, associated with oncogenic signalling pathways or promotor proximal to SEs. Although some studies indicate that these oncogenic networks are particularly sensitive due to reduction of the CR TFs within SE and promotor regions, whether down-regulation of TFs and SE-driven transcription were causally linked remained unclear (43–45). Our data indicates that targeting of SE-driven transcription is only possible when the associated gene encodes short-lived mRNA, and therefore highlights the importance of mRNA decay rates in the selective perturbation of SE oncogenic programs. This further shows that the selectivity of small molecules that can acutely affect transcription needs careful interpretation and suggests that oncogenic networks driven by SEs and short-lived and highly produced CR TFs are generally sensitized to any form of transcription inhibition, thus challenging the notion that selective targeting is required to specifically disrupt oncogenic transcription. In contrast, genes with stable mRNAs are largely refractory to transcriptional targeting on the total mRNA level, even though nascent transcriptional output is clearly reduced, and these genes tend to be functionally related to cellular housekeeping roles (29,46). This may prove a challenge for the use of transcriptional inhibitors as a therapeutic intervention for leukaemias that exhibit dysregulated metabolic activity or a heightened dependence on metabolic pathways.

Outside of cancer therapy, transcriptional and epigenetic inhibitors have been employed as immunomodulatory and anti-inflammation agents. This includes as therapies to reduce PD-L1 expression and promote host anti-tumour responses (47,48), downregulate cytokine signalling pathways such as NFkB and TGF-β in rheumatic diseases (49–52) and repress pro-survival apoptotic proteins in arthritis (53). In addition to their tumour intrinsic effects, transcriptional and epigenetic inhibitors also impact immune cells and their microenvironment directly (54,55). Similar to our observations in tumour cell targeting, RNA half-life may have a significant role in determining the therapeutic outcome of transcriptional and epigenetic compounds in the aforementioned diseases contexts. Moreover, as RBPs such as ELAVL1 are similarly important for stabilizing transcripts to drive inflammatory phenotypes (56), dual transcription and RNA decay targeting may prove useful for improving therapeutic outcomes.

Interestingly, alterations in mRNA decay frequently occur in cancer, including leukaemias, in either a gene-specific manner or through mutations in mRNA complexes that affect global mRNA turnover (57–62). For example, stabilization and the resultant increase in steady state expression of the

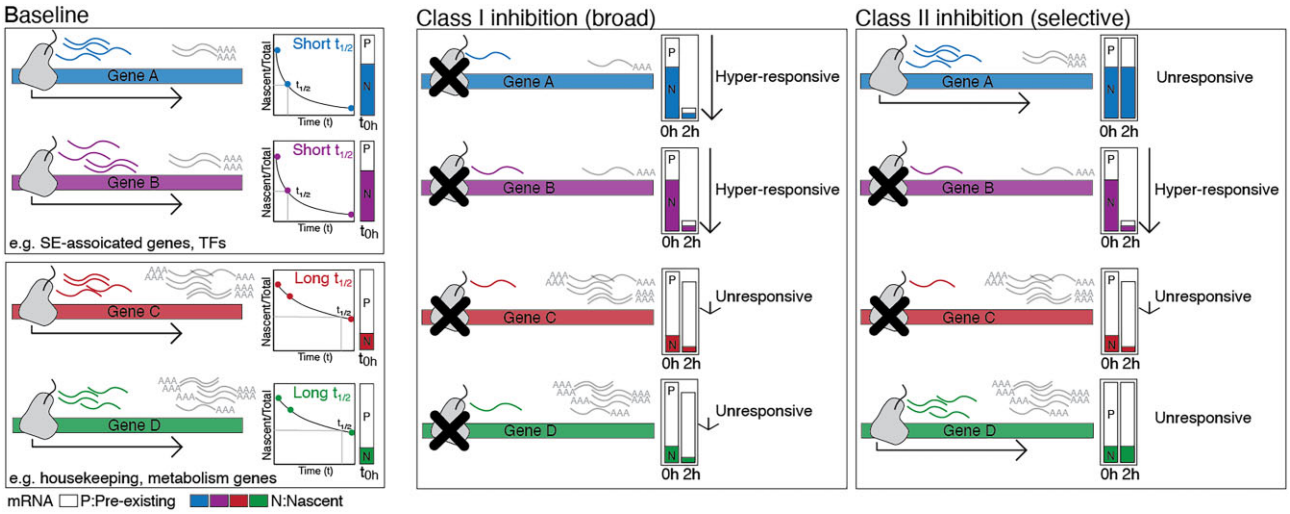

Figure 6. Simplified schematic of transcriptional responses of genes with short and long RNA half-lives with selective and broad inhibitors.

PD-L1 transcript frequently occurs in haematological and stomach cancers from mutations that disrupt the *PD-L1* 3′UTR, and in *in vivo* models of lymphoma, leads to immune evasion and decreased survival (57). Similarly, c-MYC 3′UTR truncations caused by chromosomal translocations in human T-cell leukaemias (TCL) have been described to increase c-MYC expression via transcript stabilization (61,62). Our experiments stabilizing c-MYC indicate that targeting transcription in this context nonetheless has anti-leukaemia effects, suggesting that c-MYC target genes are likely short-lived and are similarly important for driving leukemogenesis. In addition to gene-specific truncations of 3′UTR sequences in cancer, mRNA stability can be broadly affected via genetic alterations that impact the mRNA decay machinery and RBPs. This includes loss of function mutations in the carbon catabolite repression-negative on TATA-less (CCR4-NOT) transcription subunit 3 (CNOT3) subunit of the CCR4-NOT deadenylase complex in T-cell acute lymphoblastic leukaemia (T-ALL) (59) and the 3′-5′ exoribonuclease of the exosome complex, DIS3 in MM (60). Moreover, widespread alternative polyadenylation (APA) in a variety of cancer types has been demonstrated to shorten 3′UTRs and increase transcript stability and protein levels (58,63). Whilst the mechanism of increased APA in cancers is poorly understood, there is evidence that the down-regulation of APA factors such as CFIm25 and PCF11 may contribute to increased APA in certain malignancies (64). Based on our observations that long-lived transcripts are resistant to transcriptional inhibition, targeting stabilized oncogenic mRNA in the context of deregulated decay machinery may prove unsuccessful with class I and II therapeutic compounds.

Due to the lack of on-target inhibitors, therapeutic inhibition of mRNA decay pathways in the oncology setting remains largely unexplored. The widely utilized chemotherapeutic nucleoside analog 5-flurouracil (5-FU), initially characterized to perturb the DNA synthesis regulator thymidylate synthase, has also been reported to perturb the exosome subunit EXOSC10 (65,66). Moreover, small molecule inhibition of the scavenger mRNA de-capping enzyme DCPS using RG3039 in pre-clinical AML models affected pre-mRNA splicing, rather than cytoplasmic decay pathways to elicit cytotoxic effects (67). An alternative approach to alter transcript decay in cancer for therapeutic benefit has been to target RBPs that promote oncogenic mRNA stability. In the leukaemia setting, recent work has demonstrated that the ELAVL1 inhibitor MS-444 destabilizes the mitochondrial import protein TOMM34 and hampers LSC-driven leukaemic reconstitution without affecting normal blood cell populations *in vivo* (14). In line with these findings, we observe that genetic knockout and therapeutic inhibition of ELAVL1 limits THP-1 cell line growth. Targeting mRNA decay pathways directly or through RBPs is of high clinical significance, particularly because long-lived transcripts not amenable to transcriptional inhibition encode for proteins that regulate cellular homeostasis and metabolism. Indeed, aberrant metabolism is recognized as a cancer hallmark and is central to leukaemia cell survival and proliferation (68,69). This is supported by pre-clinical studies in leukaemia models showing that small molecule inhibition of various metabolic pathways as a highly promising avenue for leukaemia therapy (69). Efforts to destabilize long-lived mRNAs may therefore be an alternative approach to perturb oncogenic metabolism.

Having observed that many mRNAs are not sensitive to transcriptional perturbation due to their long half-lives, we demonstrated that combination therapy with a transcript destabilizing agent such as MS-444, provides a novel opportunity to target genes that were otherwise impervious to RNAPII targeting. Whilst we demonstrated that several transcripts were significantly sensitized with ELAVL1 knockout or MS-444 treatment upon CDK9i treatment, only a minority possessed long half-lives. As knockout of ELAVL1 has been demonstrated to alter mRNA decay rates, our half-life measurements, derived from THP-1 cells with wild-type ELAVL1, may under-estimate the number of transcripts with short mRNA decay kinetics (56). Alternatively, as the genetic screens revealed several RPBs that control fate beyond RNA decay, such as splicing, export and capping, similarly sensitize cells to CDK9i (Figure 5A), ELAVL1 may potentially affect other aspects of RNA fate. Indeed, ELAVL1 knockout in leukaemic stem cell populations has been demonstrated to globally alter splicing (14).

Overall, this study highlights the importance of mRNA decay rates in governing total gene expression levels in response to selective and global inhibitors of RNAPII-driven transcrip-

tion and provides novel mechanistic insight that can be leveraged for therapeutic benefit. Moreover, our work shifts the paradigm that selective responses observed in these contexts are largely driven by chromatin determinants such as SEs, and instead suggest that this is a result of mRNA kinetics.

Data availability

The accession number for the next generation sequencing data reported in this paper is Gene Expression Omnibus: GSE229314.

Supplementary data

Supplementary Data are available at NAR Cancer Online.

Acknowledgements

We thank members of the Victorian Centre for Functional Genomics, Peter MacCallum Centre Molecular Genomics Core, Daniel Ho from Novartis and the other authors for their help during DRUG-seq protocol implementation and Compounds Australia at Griffith University for their provision of specialized compound management and logistics research services to the project. *Author contributions:* I.T. performed experiments, next generation sequencing analysis, data interpretation and wrote the manuscript. M.J.T. performed experiments, data analysis, and manuscript writing. B.F. and A.T.P performed next generation sequencing analysis and computational modelling. Z.F. designed sgRNA and plasmid templates for CRISPR-HDR. S.G., D.Y., G.M.A. and K.J.S. optimized and performed DRUG-seq. I.Y.K. performed Myc intracellular staining and total cell number assays and analysis and was supervised by E.D.H. S.B. performed combination therapy experiments. M.Z. performed TCGA analysis. S.J.V. and R.W.J. performed data interpretation, study supervision and co-wrote the manuscript. All co-authors proof-read and edited the manuscript.

Funding

I.T. was supported by an Australian Government Research Training Scholarship; S.J.V. was supported by a Rubicon fellowship [NWO, 019.161LW.017]; NHMRC EL1 fellowship [GNT1178339]; a CSL Centenary Fellowship and a Snow Medical Fellowship; The Kids' Cancer Project; R.W.;J. was supported by the Cancer Council Victoria, National Health and Medical Research Council of Australia (NHMRC); The Kids' Cancer Project; A.T.P. was supported by a National Health and Medical Research Council (NHMRC) Senior Research Fellowship [1116955]; B.F. and A.T.P. were supported by the Lorenzo and Pamela Galli Charitable Trust and the Galli Next Generation Discoveries Initiative. The Victorian Centre for Functional Genomics (to K.J.S.) is supported by the Australian Cancer Research Foundation (ACRF); G.M.A. is supported by a PeterMac Foundation Grant [1739]; Phenomics Australia (PA) through funding from the Australian Government's National Collaborative Research Infrastructure Strategy (NCRIS) program; Peter MacCallum Cancer Centre Foundation and the University of Melbourne Research Collaborative Infrastructure Program (MCRIP); equipment used for this work was funded by the Australian Cancer Research Foundation (ACRF, Tumour Heterogeneity Program); Victorian State Government Operational Infrastructure Support and Australian Government NHMRC Independent Research Institute Infrastructure Support; This research was supported by the Snow Medical Research Foundation [SMRF2021-SF346]. The funders were not involved in the design of the study, collection, analysis, and interpretation of the data, the writing of this report, or the decision to submit the article for publication.

Conflict of interest statement

The Johnstone laboratory receives funding support from Roche, Pfizer, BMS, Astra-Zeneca and MycRx. R.W.J. is a shareholder and consultant for MycRx.

References

1. Bradner,J.E., Hnisz,D. and Young,R.A. (2017) Transcriptional addiction in cancer. *Cell*, **168**, 629–643.
2. Bywater,M.J., Pearson,R.B., McArthur,G.A. and Hannan,R.D. (2013) Dysregulation of the basal RNA polymerase transcription apparatus in cancer. *Nat. Rev. Cancer*, **13**, 299–314.
3. Smith,E., Lin,C. and Shilatifard,A. (2011) The super elongation complex (SEC) and MLL in development and disease. *Genes Dev.*, **25**, 661–672.
4. Neelamraju,Y., Gonzalez-Perez,A., Bhat-Nakshatri,P., Nakshatri,H. and Janga,S.C. (2018) Mutational landscape of RNA-binding proteins in human cancers. *RNA Biol*, **15**, 115–129.
5. Keene,J.D. (2007) RNA regulons: coordination of post-transcriptional events. *Nat. Rev. Genet.*, **8**, 533–543.
6. Fan,X.C. and Steitz,J.A. (1998) Overexpression of HuR, a nuclear-cytoplasmic shuttling protein, increases the in vivo stability of ARE-containing mRNAs. *EMBO J.*, **17**, 3448–3460.
7. Peng,S.S., Chen,C.Y., Xu,N. and Shyu,A.B. (1998) RNA stabilization by the AU-rich element binding protein, HuR, an ELAV protein. *EMBO J.*, **17**, 3461–3470.
8. Nabors,L.B., Gillespie,G.Y., Harkins,L. and King,P.H. (2001) HuR, a RNA stability factor, is expressed in malignant brain tumors and binds to adenine- and uridine-rich elements within the 3′ untranslated regions of cytokine and angiogenic factor mRNAs. *Cancer Res.*, **61**, 2154–2161.
9. Mukherjee,N., Corcoran,D.L., Nusbaum,J.D., Reid,D.W., Georgiev,S., Hafner,M., Ascano,M. Jr., Tuschl,T., Ohler,U. and Keene,J.D. (2011) Integrative regulatory mapping indicates that the RNA-binding protein HuR couples pre-mRNA processing and mRNA stability. *Mol. Cell*, **43**, 327–339.
10. Bakheet,T., Hitti,E., Al-Saif,M., Moghrabi,W.N. and Khabar,K.S.A. (2018) The AU-rich element landscape across human transcriptome reveals a large proportion in introns and regulation by ELAVL1/HuR. *Biochim. Biophys. Acta Gene Regul. Mech.*, **1861**, 167–177.
11. Radich,J.P., Dai,H., Mao,M., Oehler,V., Schelter,J., Druker,B., Sawyers,C., Shah,N., Stock,W., Willman,C.L., *et al.* (2006) Gene expression changes associated with progression and response in chronic myeloid leukemia. *Proc. Natl. Acad. Sci. U.S.A.*, **103**, 2794–2799.
12. Calin,G.A., Cimmino,A., Fabbri,M., Ferracin,M., Wojcik,S.E., Shimizu,M., Taccioli,C., Zanesi,N., Garzon,R., Aqeilan,R.I., *et al.* (2008) MiR-15a and miR-16-1 cluster functions in human leukemia. *Proc. Natl. Acad. Sci. U.S.A.*, **105**, 5166–5171.
13. Topisirovic,I., Siddiqui,N., Orolicki,S., Skrabanek,L.A., Tremblay,M., Hoang,T. and Borden,K.L. (2009) Stability of eukaryotic translation initiation factor 4E mRNA is regulated by HuR, and this activity is dysregulated in cancer. *Mol. Cell. Biol.*, **29**, 1152–1162.
14. Vujovic,A., de Rooij,L., Chahi,A.K., Chen,H.T., Yee,B.A., Loganathan,S.K., Liu,L., Chan,D.C.H., Tajik,A., Tsao,E., *et al.*

(2023) In vivo screening unveils pervasive RNA-binding protein dependencies in leukemic stem cells and identifies ELAVL1 as a therapeutic target. *Blood Cancer Discov.*, **4**, 180–207.
15. Laham-Karam,N., Pinto,G.P., Poso,A. and Kokkonen,P. (2020) Transcription and translation inhibitors in cancer treatment. *Front. Chem.*, **8**, 276.
16. Villicana,C., Cruz,G. and Zurita,M. (2014) The basal transcription machinery as a target for cancer therapy. *Cancer Cell Int.*, **14**, 18.
17. Winter,G.E., Buckley,D.L., Paulk,J., Roberts,J.M., Souza,A., Dhe-Paganon,S. and Bradner,J.E. (2015) Drug development. Phthalimide conjugation as a strategy for in vivo target protein degradation. *Science*, **348**, 1376–1381.
18. Lasko,L.M., Jakob,C.G., Edalji,R.P., Qiu,W., Montgomery,D., Digiammarino,E.L., Hansen,T.M., Risi,R.M., Frey,R., Manaves,V., *et al.* (2017) Discovery of a selective catalytic p300/CBP inhibitor that targets lineage-specific tumours. *Nature*, **550**, 128–132.
19. Martin,R.D., Hebert,T.E. and Tanny,J.C. (2020) Therapeutic targeting of the general RNA polymerase II transcription machinery. *Int. J. Mol. Sci.*, **21**, 7–15.
20. Bensaude,O. (2011) Inhibiting eukaryotic transcription: which compound to choose? How to evaluate its activity?*Transcription*, **2**, 103–108.
21. Abedin,S.M., Boddy,C.S. and Munshi,H.G. (2016) BET inhibitors in the treatment of hematologic malignancies: current insights and future prospects. *Onco Targets Ther*, **9**, 5943–5953.
22. Neumayr,C., Haberle,V., Serebreni,L., Karner,K., Hendy,O., Boija,A., Henninger,J.E., Li,C.H., Stejskal,K., Lin,G., *et al.* (2022) Differential cofactor dependencies define distinct types of human enhancers. *Nature*, **606**, 406–413.
23. Muhar,M., Ebert,A., Neumann,T., Umkehrer,C., Jude,J., Wieshofer,C., Rescheneder,P., Lipp,J.J., Herzog,V.A., Reichholf,B., *et al.* (2018) SLAM-seq defines direct gene-regulatory functions of the BRD4-MYC axis. *Science*, **360**, 800–805.
24. Zuber,J., Shi,J., Wang,E., Rappaport,A.R., Herrmann,H., Sison,E.A., Magoon,D., Qi,J., Blatt,K., Wunderlich,M., *et al.* (2011) RNAi screen identifies Brd4 as a therapeutic target in acute myeloid leukaemia. *Nature*, **478**, 524–528.
25. Delmore,J.E., Issa,G.C., Lemieux,M.E., Rahl,P.B., Shi,J., Jacobs,H.M., Kastritis,E., Gilpatrick,T., Paranal,R.M., Qi,J., *et al.* (2011) BET bromodomain inhibition as a therapeutic strategy to target c-Myc. *Cell*, **146**, 904–917.
26. Dawson,M.A., Prinjha,R.K., Dittmann,A., Giotopoulos,G., Bantscheff,M., Chan,W.I., Robson,S.C., Chung,C.W., Hopf,C., Savitski,M.M., *et al.* (2011) Inhibition of BET recruitment to chromatin as an effective treatment for MLL-fusion leukaemia. *Nature*, **478**, 529–533.
27. Shi,J., Whyte,W.A., Zepeda-Mendoza,C.J., Milazzo,J.P., Shen,C., Roe,J.S., Minder,J.L., Mercan,F., Wang,E., Eckersley-Maslin,M.A., *et al.* (2013) Role of SWI/SNF in acute leukemia maintenance and enhancer-mediated Myc regulation. *Genes Dev.*, **27**, 2648–2662.
28. Winter,G.E., Mayer,A., Buckley,D.L., Erb,M.A., Roderick,J.E., Vittori,S., Reyes,J.M., di Iulio,J., Souza,A., Ott,C.J., *et al.* (2017) BET bromodomain proteins function as master transcription elongation factors independent of CDK9 recruitment. *Mol. Cell*, **67**, 5–18.
29. Herzog,V.A., Reichholf,B., Neumann,T., Rescheneder,P., Bhat,P., Burkard,T.R., Wlotzka,W., von Haeseler,A., Zuber,J. and Ameres,S.L. (2017) Thiol-linked alkylation of RNA to assess expression dynamics. *Nat. Methods*, **14**, 1198–1204.
30. Parua,P.K., Booth,G.T., Sanso,M., Benjamin,B., Tanny,J.C., Lis,J.T. and Fisher,R.P. (2018) A Cdk9-PP1 switch regulates the elongation-termination transition of RNA polymerase II. *Nature*, **558**, 460–464.
31. Mertz,J.A., Conery,A.R., Bryant,B.M., Sandy,P., Balasubramanian,S., Mele,D.A., Bergeron,L. and Sims,R.J. 3rd (2011) Targeting MYC dependence in cancer by inhibiting BET bromodomains. *Proc. Natl. Acad. Sci. U.S.A.*, **108**, 16669–16674.
32. Federation,A.J., Polaski,D.R., Ott,C.J., Fan,A., Lin,C.Y. and Bradner,J.E. (2018) Identification of candidate master transcription factors within enhancer-centric transcriptional regulatory networks. bioRxiv doi: https://doi.org/10.1101/345413, 12 June 2018, preprint: not peer reviewed.
33. Yamada,T. and Akimitsu,N. (2019) Contributions of regulated transcription and mRNA decay to the dynamics of gene expression. *Wiley Interdiscip. Rev. RNA*, **10**, e1508.
34. Schwalb,B., Michel,M., Zacher,B., Fruhauf,K., Demel,C., Tresch,A., Gagneur,J. and Cramer,P. (2016) TT-seq maps the human transient transcriptome. *Science*, **352**, 1225–1228.
35. Schofield,J.A., Duffy,E.E., Kiefer,L., Sullivan,M.C. and Simon,M.D. (2018) TimeLapse-seq: adding a temporal dimension to RNA sequencing through nucleoside recoding. *Nat. Methods*, **15**, 221–225.
36. Wu,Q., Medina,S.G., Kushawah,G., DeVore,M.L., Castellano,L.A., Hand,J.M., Wright,M. and Bazzini,A.A. (2019) Translation affects mRNA stability in a codon-dependent manner in human cells. *eLife*, **8**, 3.
37. Yeilding,N.M., Rehman,M.T. and Lee,W.M. (1996) Identification of sequences in c-myc mRNA that regulate its steady-state levels. *Mol. Cell. Biol.*, **16**, 3511–3522.
38. Lal,A., Navarro,F., Maher,C.A., Maliszewski,L.E., Yan,N., O'Day,E., Chowdhury,D., Dykxhoorn,D.M., Tsai,P., Hofmann,O., *et al.* (2009) miR-24 inhibits cell proliferation by targeting E2F2, MYC, and other cell-cycle genes via binding to "seedless" 3′UTR microRNA recognition elements. *Mol. Cell*, **35**, 610–625.
39. Sachdeva,M., Zhu,S., Wu,F., Wu,H., Walia,V., Kumar,S., Elble,R., Watabe,K. and Mo,Y.Y. (2009) p53 represses c-Myc through induction of the tumor suppressor miR-145. *Proc. Natl. Acad. Sci. U.S.A.*, **106**, 3207–3212.
40. Caput,D., Beutler,B., Hartog,K., Thayer,R., Brown-Shimer,S. and Cerami,A. (1986) Identification of a common nucleotide sequence in the 3′-untranslated region of mRNA molecules specifying inflammatory mediators. *Proc. Natl. Acad. Sci. U.S.A.*, **83**, 1670–1674.
41. Ko,C.Y., Wang,W.L., Li,C.F., Jeng,Y.M., Chu,Y.Y., Wang,H.Y., Tseng,J.T. and Wang,J.M. (2016) IL-18-induced interaction between IMP3 and HuR contributes to COX-2 mRNA stabilization in acute myeloid leukemia. *J. Leukoc. Biol.*, **99**, 131–141.
42. Blanco,F.F., Preet,R., Aguado,A., Vishwakarma,V., Stevens,L.E., Vyas,A., Padhye,S., Xu,L., Weir,S.J., Anant,S., *et al.* (2016) Impact of HuR inhibition by the small molecule MS-444 on colorectal cancer cell tumorigenesis. *Oncotarget*, **7**, 74043–74058.
43. Jia,Q., Chen,S., Tan,Y., Li,Y. and Tang,F. (2020) Oncogenic super-enhancer formation in tumorigenesis and its molecular mechanisms. *Exp. Mol. Med.*, **52**, 713–723.
44. Hnisz,D., Abraham,B.J., Lee,T.I., Lau,A., Saint-Andre,V., Sigova,A.A., Hoke,H.A. and Young,R.A. (2013) Super-enhancers in the control of cell identity and disease. *Cell*, **155**, 934–947.
45. Gryder,B.E., Wu,L., Woldemichael,G.M., Pomella,S., Quinn,T.R., Park,P.M.C., Cleveland,A., Stanton,B.Z., Song,Y., Rota,R., *et al.* (2019) Chemical genomics reveals histone deacetylases are required for core regulatory transcription. *Nat. Commun.*, **10**, 3004.
46. Schwanhausser,B., Busse,D., Li,N., Dittmar,G., Schuchhardt,J., Wolf,J., Chen,W. and Selbach,M. (2011) Global quantification of mammalian gene expression control. *Nature*, **473**, 337–342.
47. Zhu,H., Bengsch,F., Svoronos,N., Rutkowski,M.R., Bitler,B.G., Allegrezza,M.J., Yokoyama,Y., Kossenkov,A.V., Bradner,J.E., Conejo-Garcia,J.R., *et al.* (2016) BET bromodomain inhibition promotes anti-tumor immunity by suppressing PD-L1 expression. *Cell Rep.*, **16**, 2829–2837.
48. Hogg,S.J., Vervoort,S.J., Deswal,S., Ott,C.J., Li,J., Cluse,L.A., Beavis,P.A., Darcy,P.K., Martin,B.P., Spencer,A., *et al.* (2017) BET-bromodomain inhibitors engage the host immune system and regulate expression of the immune checkpoint Ligand PD-L1. *Cell Rep.*, **18**, 2162–2174.

49. Wang,K., Hampson,P., Hazeldine,J., Krystof,V., Strnad,M., Pechan,P. and J,M. (2012) Cyclin-dependent kinase 9 activity regulates neutrophil spontaneous apoptosis. *PLoS One*, **7**, e30128.
50. Klein,K. (2018) Bromodomain protein inhibition: a novel therapeutic strategy in rheumatic diseases. *RMD Open*, **4**, e000744.
51. Rossi,A.G., Sawatzky,D.A., Walker,A., Ward,C., Sheldrake,T.A., Riley,N.A., Caldicott,A., Martinez-Losa,M., Walker,T.R., Duffin,R., *et al.* (2006) Cyclin-dependent kinase inhibitors enhance the resolution of inflammation by promoting inflammatory cell apoptosis. *Nat. Med.*, **12**, 1056–1064.
52. Duan,Q., McMahon,S., Anand,P., Shah,H., Thomas,S., Salunga,H.T., Huang,Y., Zhang,R., Sahadevan,A., Lemieux,M.E., *et al.* (2017) BET bromodomain inhibition suppresses innate inflammatory and profibrotic transcriptional networks in heart failure. *Sci. Transl. Med.*, **9**, 5–7.
53. Hellvard,A., Zeitlmann,L., Heiser,U., Kehlen,A., Niestroj,A., Demuth,H.U., Koziel,J., Delaleu,N., Jan,P. and Mydel,P. (2016) Inhibition of CDK9 as a therapeutic strategy for inflammatory arthritis. *Sci. Rep.*, **6**, 31441.
54. Peeters,J.G., Vervoort,S.J., Tan,S.C., Mijnheer,G., de Roock,S., Vastert,S.J., Nieuwenhuis,E.E., van Wijk,F., Prakken,B.J., Creyghton,M.P., *et al.* (2015) Inhibition of super-enhancer activity in autoinflammatory site-derived T cells reduces disease-associated gene expression. *Cell Rep.*, **12**, 1986–1996.
55. Hogg,S.J., Beavis,P.A., Dawson,M.A. and Johnstone,R.W. (2020) Targeting the epigenetic regulation of antitumour immunity. *Nat. Rev. Drug Discov.*, **19**, 776–800.
56. Rothamel,K., Arcos,S., Kim,B., Reasoner,C., Lisy,S., Mukherjee,N. and Ascano,M. (2021) ELAVL1 primarily couples mRNA stability with the 3′ UTRs of interferon-stimulated genes. *Cell Rep.*, **35**, 109178.
57. Kataoka,K., Shiraishi,Y., Takeda,Y., Sakata,S., Matsumoto,M., Nagano,S., Maeda,T., Nagata,Y., Kitanaka,A., Mizuno,S., *et al.* (2016) Aberrant PD-L1 expression through 3′-UTR disruption in multiple cancers. *Nature*, **534**, 402–406.
58. Mayr,C. and Bartel,D.P. (2009) Widespread shortening of 3′UTRs by alternative cleavage and polyadenylation activates oncogenes in cancer cells. *Cell*, **138**, 673–684.
59. Vicente,C., Stirparo,R., Demeyer,S., de Bock,C.E., Gielen,O., Atkins,M., Yan,J., Halder,G., Hassan,B.A. and Cools,J. (2018) The CCR4-NOT complex is a tumor suppressor in Drosophila melanogaster eye cancer models. *J. Hematol. Oncol.*, **11**, 108.
60. Weissbach,S., Langer,C., Puppe,B., Nedeva,T., Bach,E., Kull,M., Bargou,R., Einsele,H., Rosenwald,A., Knop,S., *et al.* (2015) The molecular spectrum and clinical impact of DIS3 mutations in multiple myeloma. *Br. J. Haematol.*, **169**, 57–70.
61. Aghib,D.F., Bishop,J.M., Ottolenghi,S., Guerrasio,A., Serra,A. and Saglio,G. (1990) A 3′ truncation of MYC caused by chromosomal translocation in a human T-cell leukemia increases mRNA stability. *Oncogene*, **5**, 707–711.
62. Aghib,D.F. and Bishop,J.M. (1991) A 3′ truncation of myc caused by chromosomal translocation in a human T-cell leukemia is tumorigenic when tested in established rat fibroblasts. *Oncogene*, **6**, 2371–2375.
63. Xia,Z., Donehower,L.A., Cooper,T.A., Neilson,J.R., Wheeler,D.A., Wagner,E.J. and Li,W. (2014) Dynamic analyses of alternative polyadenylation from RNA-seq reveal a 3′-UTR landscape across seven tumour types. *Nat. Commun.*, **5**, 5274.
64. Yuan,F., Hankey,W., Wagner,E.J., Li,W. and Wang,Q. (2021) Alternative polyadenylation of mRNA and its role in cancer. *Genes Dis*, **8**, 61–72.
65. Kammler,S., Lykke-Andersen,S. and Jensen,T.H. (2008) The RNA exosome component hRrp6 is a target for 5-fluorouracil in human cells. *Mol. Cancer Res.*, **6**, 990–995.
66. Silverstein,R.A., Gonzalez de Valdivia,E. and Visa,N. (2011) The incorporation of 5-fluorouracil into RNA affects the ribonucleolytic activity of the exosome subunit Rrp6. *Mol. Cancer Res.*, **9**, 332–340.
67. Yamauchi,T., Masuda,T., Canver,M.C., Seiler,M., Semba,Y., Shboul,M., Al-Raqad,M., Maeda,M., Schoonenberg,V.A.C., Cole,M.A., *et al.* (2018) Genome-wide CRISPR-Cas9 screen identifies leukemia-specific dependence on a pre-mRNA metabolic pathway regulated by DCPS. *Cancer Cell*, **33**, 386–400.
68. Hanahan,D. and Weinberg,R.A. (2011) Hallmarks of cancer: the next generation. *Cell*, **144**, 646–674.
69. Rashkovan,M. and Ferrando,A. (2019) Metabolic dependencies and vulnerabilities in leukemia. *Genes Dev.*, **33**, 1460–1474.

Received: April 11, 2023. **Revised:** July 30, 2024. **Editorial Decision:** September 9, 2024. **Accepted:** September 13, 2024